ELSEVIER

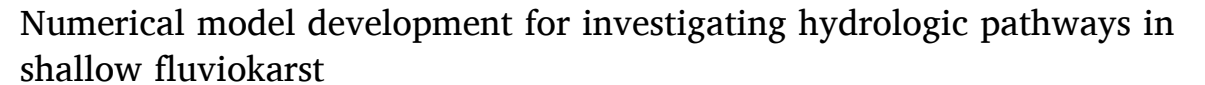
Contents lists available at ScienceDirect

Journal of Hydrology

journal homepage: www.elsevier.com/locate/jhydrol



Research papers





Nabil Al Aamery ^a, Ethan Adams ^a, James Fox ^{a,*}, Admin Husic ^b, Junfeng Zhu ^c, Morgan Gerlitz ^a, Carmen Agouridis ^d, Leonie Bettel ^a

- ^a Civil Engineering, Architectural Engineering at the Univ of Kansas, USA
- ^b Civil, Environmental, and Architectural Engineering at the Univ of Kansas, USA
- ^c Kentucky Geological Survey, USA
- ^d Biosystems and Agricultural Engineering at the Univ of Kentucky, USA

ARTICLE INFO

This manuscript was handled by C. Corradini, Editor-in-Chief

Keyword: Fluviokarst

ABSTRACT

Karst pathways and fluvial pathways control hydrology in shallow fluviokarst basins, and numerical modelling of fluviokarst is seldom reported. In this study, we developed a combined discrete-continuum fluviokarst numerical model by simulating surface river routing, in-stream swallet sources and sinks, epikarst storage and dynamic transfer, matrix bedrock interactions, and closed conduit phreatic flow. We applied the model to the Cane Run-Royal Spring basin in Kentucky, USA. Model evaluation indicated that spring discharge alone inadequately constrained model pathways and uncertainty. Instead multi-objective calibration, integrating riverine discharge and well-head data from multiple locations, assisted in identifying sensitive parameters (p < 0.05). Multiobjectives improved representation of stream-cave connectivity and limited prior knowledge biases of the system but was computationally expensive with 168 h required on a high-performance cluster. Results provided evidence for a mature fluviokarst basin with well-defined fracture-conduit network and phreatic aguifer. Residence times of karst pathways vary by five orders of magnitude, ranging from less than one hour in vertical swallets, 12.7 h in longitudinal conduits, 12.7 days in the vadose zone and epikarst, and 142.7 days in the bedrock matrix. Results suggest arrival of source waters to the subsurface systems is disconnected in time from the springflow response. Model simulations show a dimensionless vertical to longitudinal conveyance ratio helps predict swallets linking the fluvial and karst systems. Transferability of the developed model, and other karst models, is discussed relative to availability of information for karst basins.

1. Introduction

Many hydrologic pathways are possible in shallow fluviokarst basins because both fluvial and karst processes exist. Fluvial control of pathways includes runoff generation and routing of surface water whereas karst control of pathways includes density and size of sinkholes and subsurface fractures for dynamic storage and transfer of groundwater. Further, hydrologic connectivity between fluvial and karst pathways is facilitated by in-stream fluviokarst swallets, which act as vertical conveyors, connecting surface and subsurface waters at rapid timescales (see Fig. 1). The concept of the many potential hydrologic pathways of fluviokarst has taken shape in recent years (Phillips and Walls, 2004; Husic et al., 2017a, 2017b), however the complexity of pathways and their uncertain connectivity adds difficulty to predicting water budgets

and pollutant fate.

Numerical modelling of fluviokarst hydrologic processes provides one method to help fill knowledge gaps for fluviokarst. Numerical modelling of karst basins receives some criticism because models can easily become data-starved, over-parameterized, or contain deficiencies in model structure (e.g., Hartmann et al., 2014; Chang et al., 2019). Nevertheless, numerical modelling results can be useful and defendable when the model is appropriately scaled, represents known morphology and processes in the basin, has a wide variety of data, and considers all acceptable solutions during model evaluation (Hartmann et al., 2014). To remedy potential karst modelling pitfalls, it is helpful to study watersheds with extensive datasets when karst models with increased complexity are used to address knowledge gaps of processes.

We develop a combined discrete continuum numerical model for

E-mail address: james.fox@uky.edu (J. Fox).

 $^{^{\}ast}$ Corresponding author.

mature fluviokarst that simulates connectivity between surface streams and karst groundwater pathways. Combined discrete continuum models have been developed for karst systems in recent years. These models include distributed subroutines and discrete element components. The distributed subroutines follow process-based modelling of the groundwater domain and solves the governing equations with numerical methods (Hartmann et al., 2014). The discrete elements are applied to solve the governing equations for flow through discrete conduit networks (Chang et al., 2015; Qiu et al., 2019; Kayousi et al., 2020). For

example, Chang et al. (2015) and Kavousi et al. (2020) apply MODFLOW-CFP with conduit flow process subroutines to simulate groundwater drainage to conduits. Qiu et al. (2019) applied the process-based adaptive watershed simulator plus community land model (PAWS + CLM), and treated karst conduits as subsurface open channels draining the surrounding rock matrix.

To our knowledge, few, if any, studies develop a fluviokarst-specific combined discrete continuum numerical model. The model herein accomplishes this task by coupling three sub-models. An upper

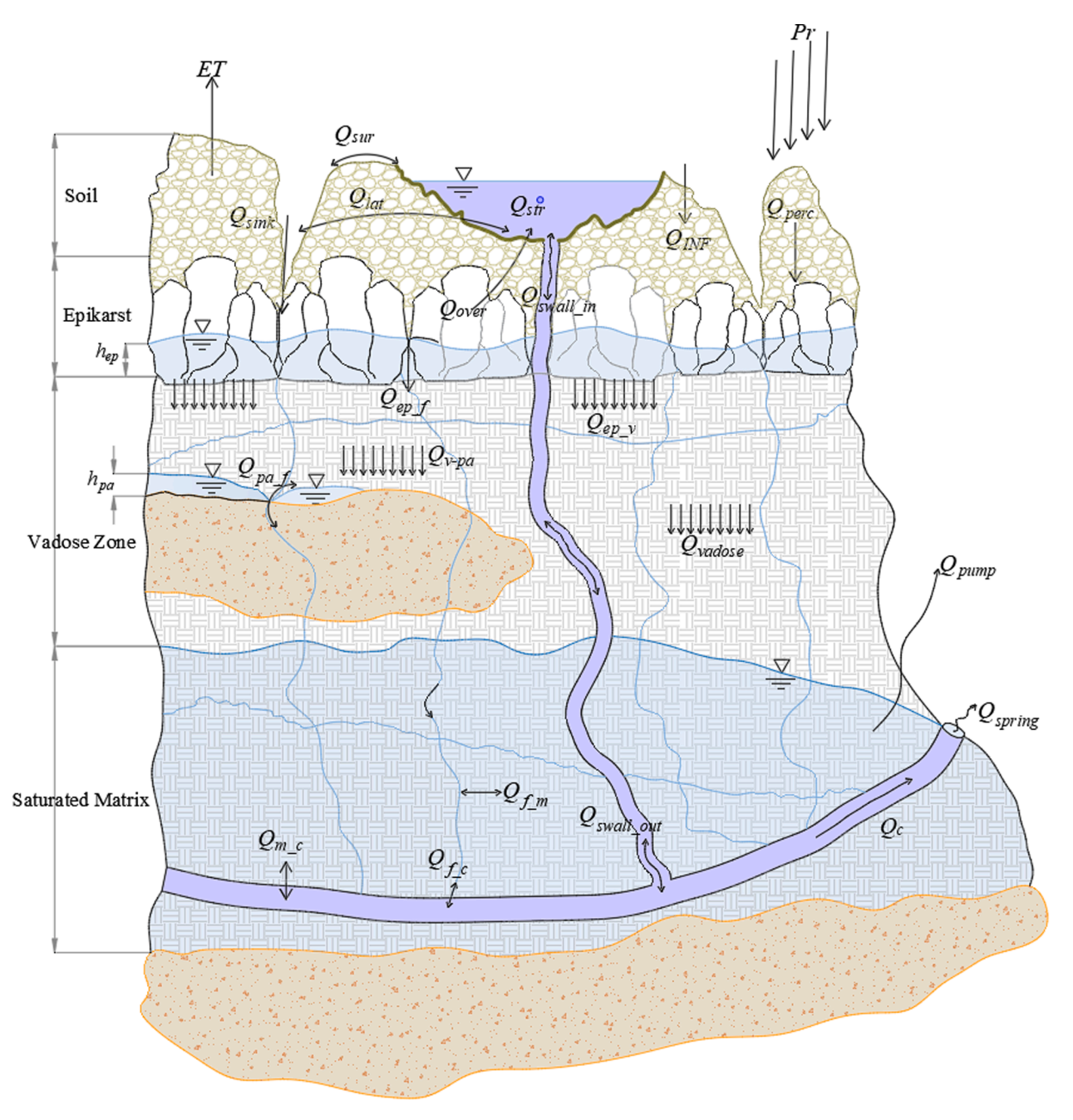


Fig. 1. Pathways in fluviokarst basins. Precipitation (*Pr*) at the land surface either infiltrates to the soil (*QINF*) or runs off to sinkholes or the stream network (*Qsur*). Soil water moves laterally to sinkholes or the stream network (*Qlat*), percolates vertically through the soil profile to the epikarst (*Qperc.*), or re-enters the atmosphere through evapotranspiration (*ET*). Stream water moves down gradient in the stream network (*Qstr*) or moves vertically to the subsurface *via* swallets (*Qswall-in*). Swallet flow reverses direction during upwelling of groundwater flow to the stream. Water stored in the epikarst percolates vertically to the vadose zone (*Qep-v*) or moves to the fracture network (*Qep-f*), where it is generally considered the latter is activated during hydrologic events and wet times of the year. Sinkhole water also moves to the fracture network (*Qsink* water stored in the vadose zone percolates as unsaturated flow (*Qvadose*) until it reaches the water table. Water in perched aquifers or phreatic matrix exchanges with fractures (*Qpa-f*) or higher porosity conduits (*Qf-c*). Depending on human population density and land uses, water leaves the aquifer via well pumping (*Qpump*). Water conveys through conduits to springs (*Qc*). During very wet conditions such as an extreme hydrologic event, fracture networks and epikarst reaches their capacity, and overflow occurs to the stream network (*Qover*), which leaves the basin via surface water outlets.

groundwater model divides the groundwater domain to sub-basins and then distributes each sub-basin vertically. A lower groundwater models solves the governing equations for discrete fractures, swallets and conduits. A surface stream model simulates the fluvial system aboveground and interacts with karst swallets. Unique features of the fluviokarst model include: the numerical treatment of swallets located in the stream corridor and the numerous conditions for which they can exist (i.e., filling, overtopping swallets, reversing flow, emptying); discrete elements for fractures, swallets and conduits; and coupling the timescales of water through the three sub-models to simulate both surface streamflow and groundwater flow across pathways. Stream routing, epikarst flows, vadose zone transport, fracture flow and conduit flow consider fluid continuity and transport formula controlling each process (Zimmerman and Yeo, 2000; Jain, 2001; Niswonger et al., 2006; Tritz et al., 2011; Rooij et al., 2013; Chen and Goldscheider, 2014). The model is evaluated quantitatively and thereafter discussed regarding multiobjective calibration needs, data inputs and parameterization needs, and computational costs.

We apply our formulated numerical model to investigate fluviokarst hydrology including aquifer structure, hydrologic pathways, and instream swallet features. Knowledge of aquifer structure for fluviokarst can add understanding of the spectrum of karst matrix and its features, such as characterizing fracture-conduit permeability and rock matrix permeability (e.g., Matthäi and Belayneh, 2004). Hydrologic pathways in fluviokarst are hypothesized to show their imprint on springflow analogous to karst basins with little to no fluvial influence. For example, karst hydrologists often separate springflow into quick-, intermediateand slow-flow pathways (Baedke and Krothe, 2001; Kovács and Perrochet, 2008; Fiorillo, 2011), but extension of these concepts to fluviokarst basins is less clear. In-stream swallet features are a defining morphology of fluviokarst basins, and in-stream swallets are hypothesized to pirate surface streamflow to karst aquifers during some conditions and reverse flow from the aquifer to the surface during other conditions (Chen and Goldscheider, 2014; Hensley et al., 2014). However, investigation of the in-stream swallets is seldom reported, which is likely due to difficulties in collecting measurements around the swallets and numerically coupling streamflow models with swallet flow and fracture-conduit flow models.

To summarize, the objectives of this paper were to: (i) develop and evaluate a numerical model for shallow fluviokarst and report the model's input and calibration needs, advantages and limitations; and (ii) use the model to investigate fluviokarst hydrology including aquifer structure, hydrologic pathways, and in-stream swallet features. Discussion of these goals provides the sub-headings for the discussion section of the paper.

2. Model formulation

The fluviokarst model simulates the hydrologic pathways defined and depicted for fluviokarst in Fig. 1. Some pathways are one-way pathways, such as runoff and fracture overflow to the surface stream, while many of the pathways are simulated to occur in either direction depending on hydraulics, such fractures recharging the rock matrix or the rock matrix discharging to fractures. The fluviokarst pathways and their possible directions are shown in Fig. 2. To accomplish the pathway simulation, the formulation includes a surface stream model, an upper groundwater model, a lower groundwater model, and numerical optimization. The model formulation assumes external inputs to the model, either from measurements or independent models, including fluxes for soil water percolation to the epikarst, runoff and lateral flow to the surface stream network, and runoff and lateral flow entering land surface sinkholes (see model workflow schematic in Fig. S1). The model formulation is currently limited to shallow, epigenetic fluviokarst and we do not account for hypogenic recharge.

2.1. Surface stream model

The surface stream model is formulated to route water through the stream network and account for water exchange with the lower groundwater model *via* fluviokarst swallets located in the stream

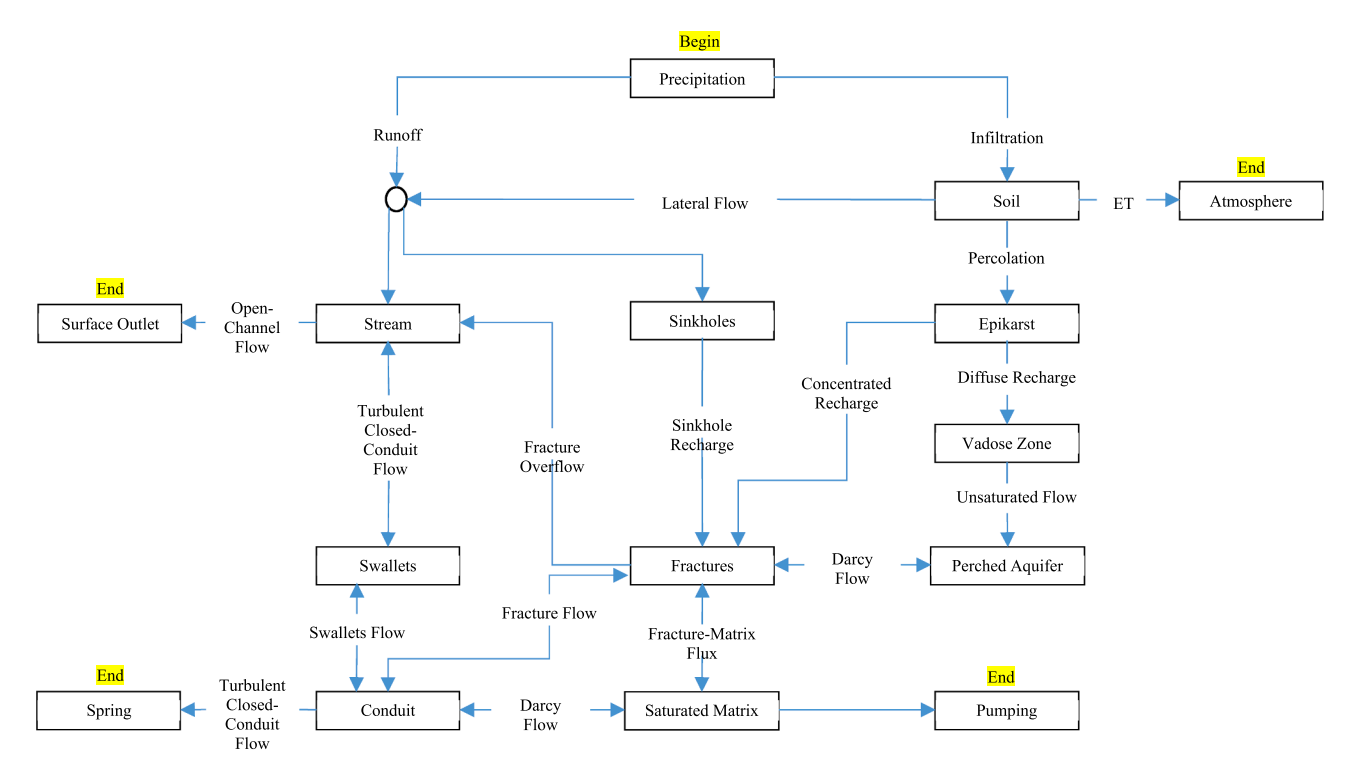


Fig. 2. Fluviokarst pathways diagram simulated with the developed model. The arrows show how some pathways are one-directional, such precipitation goes to runoff and runoff goes to the stream or to sinkholes. Other arrows show twodirectional as possible, such as exchange from the fractures to the rock matrix and visa versa.

corridor (see Fig. 1). Stream reach continuity is

$$\frac{dV_{str}}{dt} = Q_{str-up} + Q_{sur} + Q_{trib} + Q_{lat} - Q_{swall-in} - Q_{str-dn}$$
(1)

where V_{str} is the volume of water stored in a stream reach; Q_{str-up} and Q_{str-dn} are water transferred in and out of the reach; Q_{str} , Q_{trib} , and Q_{lat} are lateral inputs to the stream from surface runoff, tributaries considered external to the network, and lateral soil flow, respectively. $Q_{swall-in}$ is exchange between the surface stream and the lower groundwater model, and the swallet flux is shown as a sink in Eq (1) but can be a source term for swallet reversal. Q_{str} , Q_{trib} , and Q_{lat} are model inputs. Q_{str-up} and Q_{str-dn} are formulated using Mannings' equation and Jones' formula to account for non-uniformity in the model (Chow, 1959; Jain, 2001). $Q_{swall-in}$ is input from the lower groundwater model.

2.2. Upper groundwater model

The upper groundwater model simulates water storage and transfer for the epikarst, unsaturated rock matrix, and saturated rock. Epikarst continuity is

$$\frac{dV_{ep}}{dt} = Q_{perc} - Q_{ep-v} - Q_{ep-f}, \tag{2}$$

where V_{ep} is the volume of water stored in the epikarst; t is time; Q_{perc} is soil water percolation input to the epikarst; Q_{ep-v} is water transfer out of the epikarst to the vadose rock zone; and Q_{ep-f} is water transfer out to the fracture network. Q_{perc} is a model input, and Q_{ep-v} is solved for in the vadose zone routing. Q_{ep-f} is modelled using the formulation of Tritz et al. (2011) and occurs when an activation threshold height is exceeded as

$$q_{ep-f} = \left[\left(h_{ep} - h_{epth} \right) n_{ep} \right] \Delta t^{-1} \text{for} h_{ep} > h_{epth}, \text{else} q_{ep-f} = 0$$
(3)

where q_{ep} is water discharge per unit area, h_{ep} is the height of water stored in the epikarst; h_{epth} is the threshold height when epikarst water will be routed to the fracture network; and n_{ep} is the epikarst porosity. Using the formulation of Eq. (3), an overflow is activated when the threshold is reached in the epikarst layer. This approach is conceptually consistent with the model by Tritz et al. (2011). The epikarst transfers water vertically to the rock matrix (i.e., vadose zone) below but also includes a threshold such that water can overflow to the fracture network. This is consistent with a near surface layer that is interconnected with fractures. Lateral flow is not considered explicitly, however, the fracture network grid is three dimensional and in a given time step immediately removes overflow to the fracture network.

Vadose rock matrix is represented as a variably saturated granular rock entering from the epikarst and exiting to saturated rock. Multilayered water content is formulated with Richard's Equation assuming flow is gravity driven so the diffusive term can be removed (Simunek et al., 1998; Niswonger et al., 2006) and formulating hydraulic conductivity with the Brooks-Corey function as

$$\frac{d\theta}{dt} = \frac{d}{dz} [-K(\theta)] \tag{4}$$

$$K(\theta) = K_s \left[\frac{\theta - \theta_r}{\theta_s - \theta_r} \right]^{\epsilon}$$
 (5)

where θ is the volumetric water content; z is the vertical soil depth; $K(\theta)$ is the hydraulic conductivity as a function of θ ; K_s is the saturated hydraulic conductivity of the rock mass; θ_r and θ_s are is the residual and saturated volumetric water content of the rock mass; and ϵ is the Brooks-Corey exponent. The product of the groundwater cell area and the hydraulic conductivity solved for at the boundaries provides fluxes from the epikarst to the vadose zone and vadose zone to saturated matrix (i.e., $Q_{ep-\nu}$ and $Q_{\nu-pa}$).

Saturated rock in the upper groundwater model is used to represent the presence of aquitards that produce perched water tables, and continuity for the saturated rock is

$$\frac{dV_{pa}}{dt} = Q_{v-pa} - Q_{pa-f} \tag{6}$$

where V_{pa} is the volume of water stored in a perched aquifer; Q_{v-pa} is vadose zone input to the perched aquifer; and Q_{pa-f} is the exchange flow between the perched aquifer and fracture network. The latter is formulated with Darcy's law as

$$q_{pa-f} = K_s \frac{dh}{dx} \tag{7}$$

where dh is the difference in elevation of the saturated rock head and fracture network head; dh and q_{pa-f} are negative when the fracture head is higher than the perched saturated rock; and dx is the flow path distance and is a function of spacing between fractures.

2.3. Lower groundwater model

The lower groundwater model simulates water storage and transfer for the fracture network, swallets, the conduit network, and the lower saturated matrix. The fracture network is represented as plate-like void spaces in the rock, and continuity is

$$\frac{dV_f}{dt} = Q_{sink} + Q_{ep-f} + Q_{pa-f} - Q_{f-c} - Q_{f-m} - Q_{over}$$
(8)

where V_f is the volume of water stored in the fracture network; Q_{sink} is water transfer entering the fractures via land surface sinkholes; Q_{f-c} and Q_{f-m} are transfers out of the fracture network to conduit and the lower saturated rock matrix, respectively, although both terms can be negative in Eq. (8) indicating sources rather than sinks; and Q_{over} is fracture network overflow manifested as seeps and hillside springs in karst terrain. Q_{f-c} is formulated with the cubic law for fracture flow (Snow, 1969; Long et al., 1985; Bear et al., 2012; Zimmerman and Yeo, 2000) as

$$q_{f-c} = \frac{\rho g}{6\mu} \frac{dh}{dx} Nb^3 \tag{9}$$

where ρ is water density; g is gravity; μ is viscosity; $\frac{dh}{dx}$ is the hydraulic gradient; and Nandb are fracture density and aperture. Q_{f-m} is formulated with Darcy's law similarly to Eq. (7). Q_{over} is formulated for the condition when the hydraulic head of the fracture is greater than the epikarst threshold height, $(h_f > h_{epth})$ because this indicates both the epikarst and fractures are full, as

$$q_{over} = q_{ep-f} + \left[\left(h_f - h_{epth} \right) 3Nb \right] \Delta t^{-1}$$
(10)

The fluviokarst swallets and phreatic conduits are represented using a network of subterranean pipes approach (Jeannin, 2001; Shoemaker et al., 2008; Rooij et al., 2013; Chen and Goldscheider, 2014). Swallets and conduits are formulated as equivalent-diameter, tortuous cylindrical segments, and continuity is

$$\frac{dV_s}{dt} = Q_{swall-in} - q_s A_s \tag{11}$$

$$\frac{dV_c}{dt} = Q_{c-up} + q_s A_s + Q_{f-c} + Q_{m-c} - Q_{c-dn}$$
 (12)

where V_s and V_c are the volume of water in the swallet and conduit segments; q_s and A_s are the swallet velocity and area; and Q_{c-up} and Q_{c-dn} are the upstream and downstream fluxes to the conduit segment. $Q_{swall-in}$ is defined in Eq. (1) and is formulated with a weir equation (e.g., Gupta, 2016) when the swallet is not full. When the swallet is full, the free surface of the stream is the swallet head, $Q_{swall-in} = q_s A_s$, and is solved for as part of the lower groundwater model. In Eq. (12), Q_{m-c} is

exchange between the lower saturated matrix and conduit and is formulated with Darcy's law similarly to Eq. (7). The swallet-conduit network is formulated using the nodal approach as

$$\Delta E = \pm f_{s,c} \frac{I_{s,c} \tau_{s,c}}{D_{s,c}} \frac{(q_{s,c})^2}{2g}$$
 (13)

where ΔE is the energy difference across a swallet (s) or conduit (c); f is the friction factor;D and l are diameter and length of the segment; and τ is tortuosity of the swallet or conduit.

The lower saturated matrix is formulated similarly as the upper matrix as variable-volume storage with a lower permeability than fractures and conduits (White, 1999; Hartmann et al., 2013), and continuity is

$$\frac{dV_m}{dt} = Q_{vadose} - Q_{m-c} - Q_{pump} \tag{14}$$

where V_m is the volume of water in the matrix.

2.4. Numerical formulation

The numerical formulation uses a combined discrete-continuum approach. The groundwater-surface water basin is divided to spatial grids. Surface stream networks, swallets, and conduits are modeled discretely. The epikarst, fracture network, unsaturated zone, and saturated matrix are modeled as continuums.

At each time step, the surface stream model, upper groundwater model, and lower groundwater model are solved following the method in Fig. 3. The surface stream network is solved at each time step using flood wave routing considering non-uniform flow (Jain, 2001) and surface inputs from runoff and lateral flow. Transfer with the lower groundwater model is solved either using weir equations or solved in the lower groundwater model depending on whether the swallets are partially full or full, respectively.

The upper groundwater model is solved for each groundwater cell considering input from soil percolation. The model calculates the number of vadose layers in the vertical so the CFL condition will not be violated and solves the Richards' equation through iteration for the discretized cells (e.g., Simunek et al., 1998; Niswonger et al., 2006). Output from the upper groundwater model include exchanges for epikarst to fractures and saturated matrix to fractures, and these fluxes are inputs to the lower groundwater model during each time step.

The lower groundwater model simultaneously solves a system of equations setup across all discretized groundwater cells for each time step with inputs from the stream model and upper groundwater model for each cell. The system of equations includes an equivalent porous medium approach for the fracture network equations in each groundwater cell (Snow, 1969; Kresic, 2010), a similar continuum approach is used for the saturated matrix in each cell, and the discretized swallet and conduit nodal approach is solved across all groundwater cells. Optimization solves the system for conduit, swallet, matrix and fracture fluxes, static pressure heads in the fractures, conduits and swallets without boundary conditions, and the potentiometric surface of the saturated matrix. In some time steps, optimization is aided by boundary conditions for the swallets when they are full, conduits that daylight at springs, and a land surface elevation as a maximum fracture head when seeps and

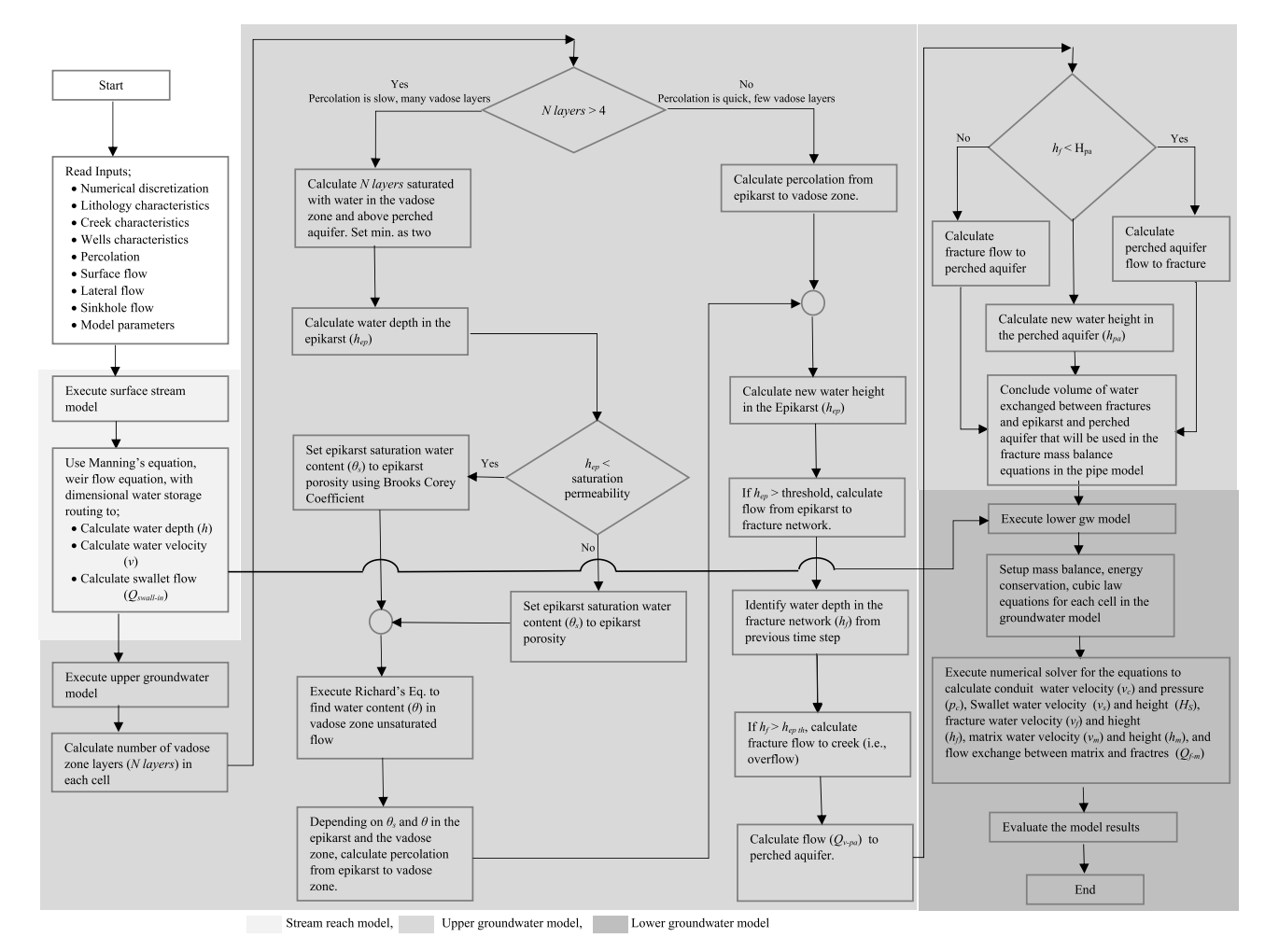


Fig. 3. Flow chart of the model. Stream reach model, Upper groundwater model, Lower groundwater model.

hillside springs occur.

Optimization of the lower groundwater model uses the trust-region with dogleg method with 1000 numerical iterations (Dennis and Schnabel, 1996). The algorithm starts with initial guesses for unknowns to define a point in the spherical trust region that adjusts size at each iteration. The initial guesses at the first time step are set intuitively, then the results assisted in defining the initial guesses for successive time steps. The tolerance is set to 1×10^{-6} during optimization method and is set to one for the two-norm of the optimized solution.

3. Model application

3.1. Study site

The Cane Run-Royal Spring fluviokarst basin in the Inner Bluegrass region of Kentucky USA was the study site for model application. The study site was chosen because: the basin classifies as mature fluviokarst with many morphologic features of epigenetic karst shown in Fig. 1 occurring to some degree; there exists many published datasets for model setup and calibration collected from tracer tests, flow gaging, LiDAR mapping, electrical resistivity mapping, well data collection, downhole videos, acoustic measurements of caves, geologic and soil surveys, water budgets, and water quality measurements (Cressman, 1967; Spangler, 1982; Thrailkill and Gouzie, 1984; Cressman and Peterson, 1986; Thrailkill et al., 1991; Drahovzal et al., 1992; Taylor, 1992; Paylor and Currens, 2004; Zhu et al., 2011; Currens et al., 2015; Sawyer et al, 2015; Tibouo, 2016; Husic et al., 2017a, 2017b, 2019a, 2019b; Bandy et al., 2019); and the basin is located just 10 km from the Kentucky Geological Survey's headquarters and the University of Kentucky.

The Cane Run Watershed (Fig. 4) is gently rolling topography with sinkholes across the landscape (Paylor and Currens 2004). The land use

is agricultural, and much of it is horse farm pasture, and urban/suburban (UKCAFE, 2018). The climate is temperate (MAT: $13.0\pm0.7\,^{\circ}$ C; MAP: $1,170\pm200\,$ mm). The soil is silt-loam. 40% of the watershed has shallow surface slopes (0–3%), 50% has moderate slopes (3–6%) and 10% has steeper slopes (>6%).

Cane Run Creek is a surface stream originating in Lexington, Kentucky and flows northwest. The stream and tributaries share most of its drainage area with Royal Spring groundwater basin (58 $\rm km^2)$ through swallets that connect surface water to the underlying karst aquifer feeding Royal Spring. >60 swallets were surveyed in Cane Run Creek (see Fig. 4). The swallet equivalent diameters at the streambed range from 10 to 100 cm. Flow pirating by the swallets causes Cane Run Creek to be dry for 90% of the year (Husic et al., 2017a).

Royal Spring karst groundwater basin is formed in Middle Ordovician aged limestones with interbeds of thin shales (Thrailkill and Gouzie, 1984; Cressman and Peterson, 1986). Epikarst features are visible throughout the watershed in naturally exposed karren as well as roadcuts (Husic et al., 2017b). Limestone members formed with high clay or silt content locally act as aquitards and were previously mapped (e.g., the Cane Run Bed, Brannon Member, Cressman, 1967; Miller, 1967; MacQuown and Dobrovolny, 1968). Water flow from the fluviokarst features and limestone bedrock converges to a phreatic conduit 15 to 20 m below the ground surface that flows northwest and surfaces at Royal Spring (Thrailkill et al., 1991; Paylor and Currens, 2004; Zhu et al., 2011). Evidence from resistivity measurements, well drilling directly intersecting the conduit and base level elevations suggest the conduit profile follows a bedding plane approximately 14 m below Cane Run Bed (Thrailkill et al., 1991; Landrum et al., 2013). Royal Spring (243 m a.s.l., mean discharge is 0.7 m³ s⁻¹) conveys perennial flow from the phreatic conduit (Currens et al., 2015).

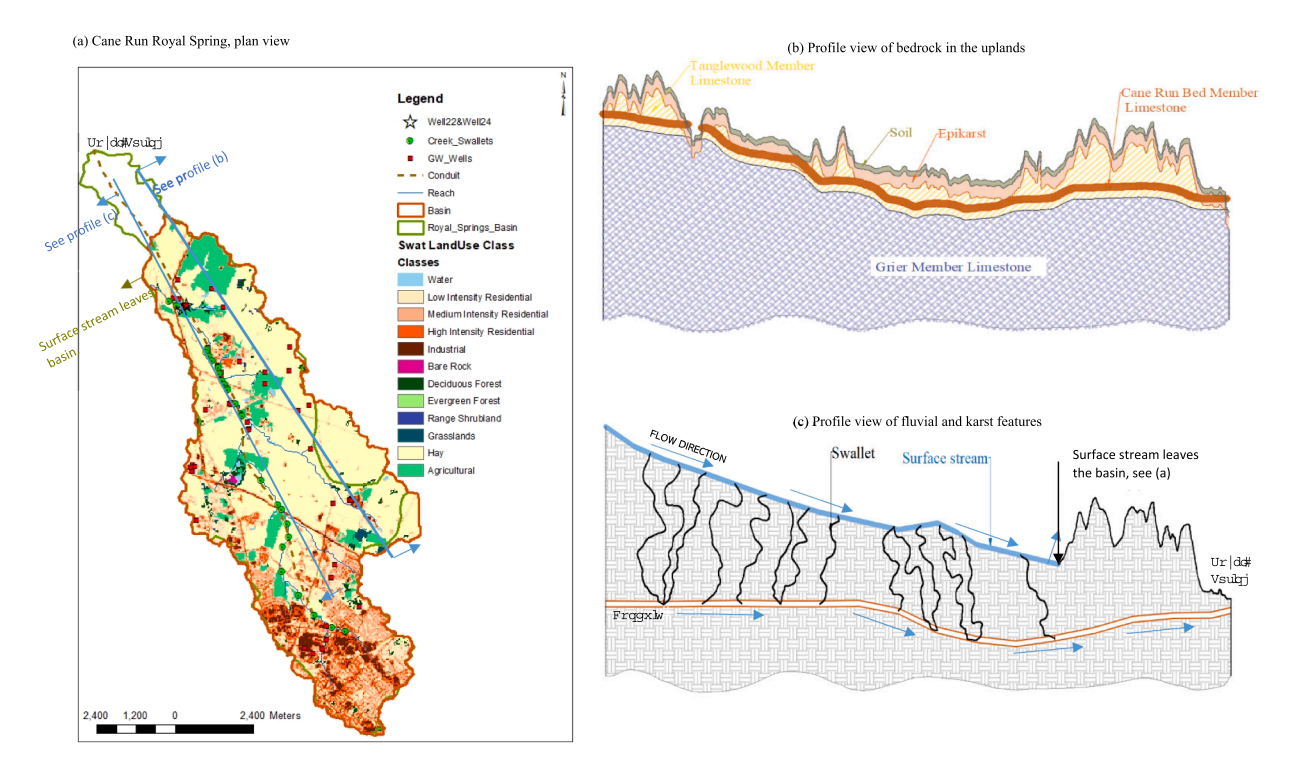


Fig. 4. Cane Run Royal Spring fluviokarst basin. (a) Plan view of the surface watershed basin and groundwater basin boundaries including in-stream fluviokarst swallets, groundwater wells and land uses throughout the basin. (b) Profile view of the bedrock structure for the uplands of the basin, located away from the main stream channel. Location of profile b is indicated in pane a. (c) Profile view of the surface stream centerline, the primary cave located 15 to 20 m below the stream, and the numerous swallets connecting the fluvial and karst members. The surface basin and groundwater basin diverge on right side of the pane. Notes: Tanglewood Member forms the upper part of the Lexington Limestone in the Bluegrass region and is calcarenite, crossbedded limestone; Cane Run Bed Member is an aquitard layer of Lexington Limestone formed with high clay or silt content locally and classify as fossiliferous shale and argillaceous limestone (Cressman, 1967; Miller, 1967; MacQuown and Dobrovolny, 1968).

3.2. Model spatial domain and inputs

The model spatial domain (see Fig. 5) was constructed using inputs detailed in Tables 1 and 2 collected from measurements in the field, geospatial data, and geology reports. Available data used included sinkhole maps, aquifer boundary maps, land use maps, stream flow network maps, soil maps, topography models, mapping of stream bathymetry, and geologic cross sections and conduit profiles.

The surface watershed (Fig. 5a) was constructed using the digital elevation model, and sinkhole maps were input to provide sinkhole locations and mapped drainage areas. Stream cross section and longitudinal dimensions were input using analyses of a 0.5 m topographic model. In-stream swallets were input using a 20 m buffer around the stream network masked over the sinkhole geospatial model. Swallet dimensions were input using data from a field survey (Puckett, 2015). The soil layer covering the limestone bedrock was mapped using digitized soil survey data. The epikarst layer was constructed immediately below the soil layer, and the epikarst thickness was input using results from soil electrical resistivity (Landrum et al., 2013).

The groundwater basin boundary followed a model constructed using groundwater tracer studies (Taylor, 1992; Paylor and Currens, 2004). The limestone bedrock layer and its fracture network were constructed below the epikarst layer and extended below the primary conduit (Fig. 5b). The geometry of fractures and density of fractures across the bedrock were left as parameters in the model because our existing resistivity measurements could not resolve these characteristics. The Cane Run Bed aquitard was input based on geologic maps and survey data, analyses of stage recordings from wells in perched aquifers, and borehole logs. The primary conduit that daylights at Royal Spring was input to follow a bedding plane approximately 14 m below the Cane Run Bed for most of its length until the local anticline near the spring (Fig. 5c). The elevation of Royal Spring was used as a maximum conduit elevation.

Discretized spatial inputs included (see Table 2): number of

Table 1
Geospatial data sources used to assist with model inputs and calibration.

Dataset	Title	Origin					
Well Locations	Water Well and Spring Location	Kentucky Groundwater					
	Map	Data Repository					
Soil	Kentucky Soil Survey	USDA Geospatial Data					
	(STATSGO)	Gateway					
Land Use	National Land Cover Dataset	USDA Geospatial Data					
	2116 Kentucky	Gateway					
30-m DEM	National Elevation Dataset 30-	USDA Geospatial Data					
	meter 37,084 Winchester &	Gateway					
	38,084 Louisville						
1.5-m DEM	Kentucky From Above 5-ft DEM	Kentucky Elevation Data					
	Tiles: N082-N089, E298-E302	and Arial Photography					
		Program					
Sinkhole Locations	LiDar Sinkholes	Kentucky Geologic Survey					
Sinkhole	GIS Sinkhole Coverage for the	Kentucky Geologic Survey					
Drainage Area	Karst Area of Kentucky	and Kentucky Speleological Survey					
Geologic Stratigraphy	24 k Structure Contours	Kentucky Geologic Survey					
Hydrography	National Hydrography Dataset	USDA Geospatial Data					
	051,002,050 Lower Kentucky	Gateway					

watershed surface cells, conduit lengths (l_c) , conduit elevation (z_c) , groundwater cell area (A_{cell}) , stream bed height relative to conduit (H_{pa}) , epikarst bottom height relative to conduit $(h_{f,max})$, maximum lateral distance for fracture and matrix flow (dx_{max}) , number of groundwater wells, number of stream reaches, stream bed width (B), stream bed slope (s), and bankfull heights (h_{bkf}) . A number of additional inputs were specified using literature. The discharge-coefficient for weir flow (c_w) into the swallet while the swallet is not full was selected based on reported broad-crested weir coefficients (Gupta, 2008). The value of the Brooks-Corey exponent (s) was assumed to be equal to the value used by Brooks and Corey (1964) in the Brooks-Corey equation. The residual

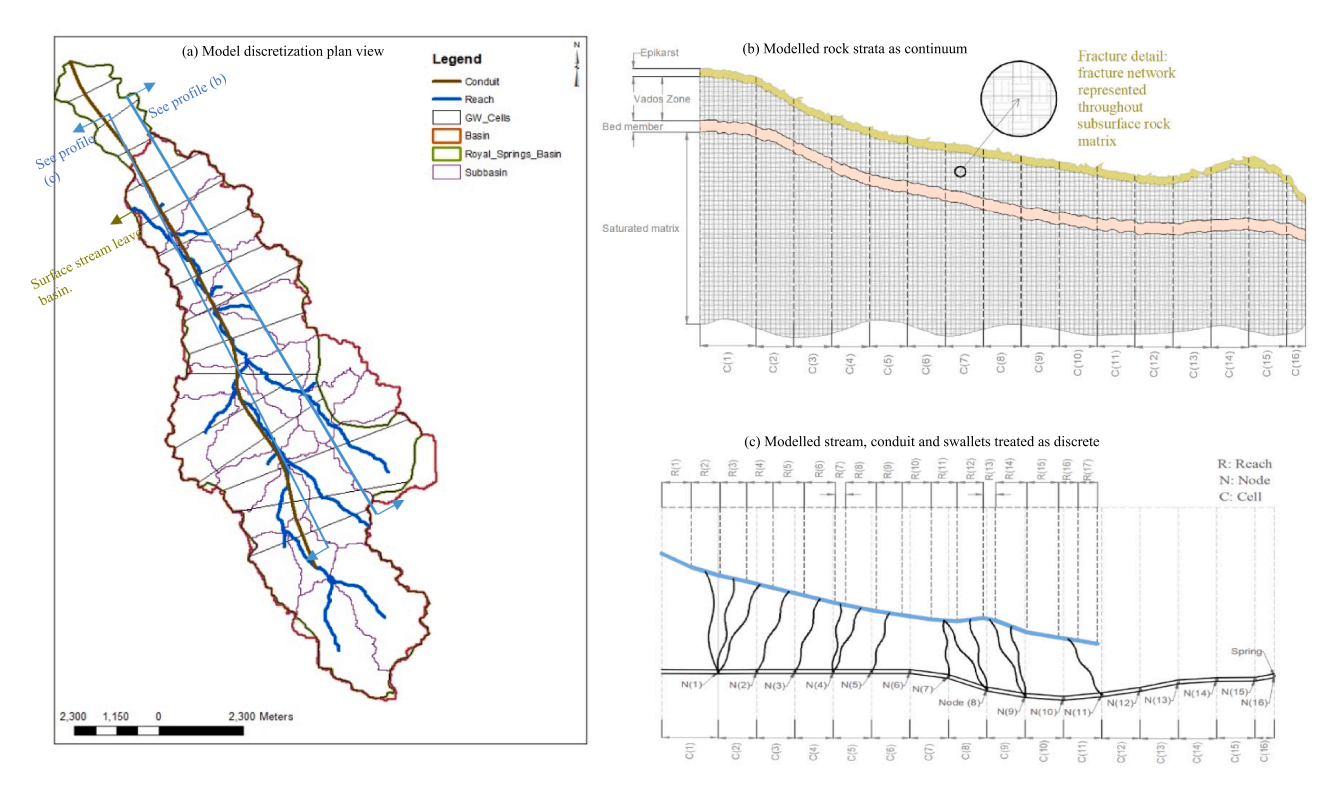


Fig. 5. Continuous discrete continuum discretization for Cane Run Royal Spring basin. (a) Plan view of surface sub-basins discretized based on topography and groundwater cells. Rock strata are treated as continuum within each groundwater cell as shown in pane (b). Reaches for the surface stream and conduit shown in pane (c) are discrete and correspond to the sub-basin and groundwater cells shown in pane (a).

Table 2Model inputs used to in application of the fluviokarst model.

Name	Symbol	Value	Units	Source
Brooks-Corey Exponent	€	4	-	Brooks and Corey 1964
Residual Moisture Content	θ_r	0	%	Simunek et al. (1998)
Gravitational Acceleration	g	9.8	m s ⁻²	Munson et al. (2013)
Density	ρ	1000	${\rm kg} \over {\rm m}^{-3}$	Munson et al. (2013)
Dynamic Viscosity	μ	0.0013	(N-s) m ⁻²	Munson et al. (2013)
Channel Side-Slope	m	2.5	$_{\mathrm{m}^{-1}}^{\mathrm{m}}$	5-ft DEM
Weir Coefficient	c_w	0.85	-	Gupta (2008)
Epikarst Thickness	H_{ep}	1	m	Landrum et al. (2013)
Number of Groundwater Cells		16	-	Assigned
Conduit Length	l_c	500-1470	m	Assigned
Conduit Elevation	z_c	235.3-244.8	m	Zhu et al. (2011)
Cell Area	A_{cell}	1.1-13.6	Km^2	Assigned
Cane Run Bed Height (perched aquifer height)	H_{pa}	9.8–37.3	m	Cressman (1967)
Epikarst Bottom Height	$h_{f,max}$	15.9–48.8	m	Landrum et al., 2013
Stratigraphic Curvature		0.03-0.29	-	Cressman, 1967
Maximum Fracture/ Matrix Lateral Distance	dx_{max}	367–1296	m	Assigned
Number of Groundwater Wells		0–8	-	Kentucky Groundwater Data Repository
Number of Stream Reaches		17	-	Assigned
Stream Bed Width	B	3.57-7.45	m	1.5-m DEM
Stream Bed Slope	s	0.0002 – 0.0055	m	1.5-m DEM
Bankfull Height	h_{bkf}	0.64-1.36	m	1.5-m DEM

moisture content (θ_r) in the unsaturated zone was assumed to be zero, as suggested by Simunek et al. (1998) to reduce the number of model parameters. The pump rate in each groundwater cell was the product of the pump rate parameter and the number of active wells in the groundwater cell identified using a geospatial dataset. Inputs for surface runoff, surface routing, and soil water percolation were estimated using the Soil Water Assessment Tool, or SWAT (Neitsch et al., 2011). SWAT's deep aquifer percolation fraction (RCHRG_DP) was set to 1 to negate the shallow aquifer and prevent baseflow to streams since these processes are simulated in the stream and groundwater code. This approach is similar to the work by Malagò et al. (2016) where SWAT surface fluxes were used as inputs to a karst groundwater model. Meteorological inputs were available from the Bluegrass Airport (NOAA ID: USW00093820).

3.3. Model parameterization

The numerical model was parameterized using 19 parameters (see Table 3). Groundwater parameter ranges for flow in limestone were considered. The initial range for the matrix porosity (n_m) was selected based on values for limestone bedrock in karst aquifers (Williams, 2008). The range for saturated hydraulic conductivity of the limestone bedrock (K_s) was selected based on minimum and maximum values of hydraulic conductivity reported for limestone bedrock by Domenico and Schwartz (1998). The range for epikarst porosity (n_{ep}) was selected based on values suggested in epikarst literature (Klimchouk, 2004; Williams, 2008). The maximum value in the initial epikarst fracture threshold height parameter (h_{epth}) was selected based on the estimated maximum thickness of the epikarst layer (Landrum et al., 2013).

We used active wells in the watershed and pumping rates for the region to help parameterize the pumping rate. We mapped the "active" wells. The locations of all wells in the groundwater basin were identified using a dataset provided by the Kentucky Geological Survey Groundwater Data Repository. This set of wells was filtered to only include active wells (see Figure below and Fig. S2 in the revised paper). Then, we parameterize pumping on what was reasonable to come from the wells in reference to pumping rate data in central Kentucky. This range of rates and number of active wells provided the initial range for the pumping rate parameter in the model (see Table 3). The maximum pump rate was selected based on high-end values of reported pumping rates from wells in the Greir Member (Carey and Stickney, 2005).

SWAT run parameter ranges for surface hydrology inputs were generated from SWAT using 25 different acceptable model runs detailed in Al Aamery et al. (2016) and Al Aamery et al. (2018). SWAT was calibrated using SWAT-CUP SUFI2 algorithm (Abbaspour et al., 2007). The algorithm is simulated and then retains acceptable model runs (i.e., R2 > 0.6). From these acceptable runs we chose 25 runs to provide the largest possible ranges and account for uncertainty propagated from SWAT through the fluviokarst model.

Additional karst groundwater and surfacewater parameter ranges were also specified. The maximum value for fracture density (N) was selected based on reported fracture densities common in epikarst zones, and the minimum value was selected based on lower end values reported for karstified limestone bedrock (Klimchouk, 2004). The range for fracture aperture (b) was selected based on a range of fracture apertures that resulted from a karst evolution model (Worthington and Ford, 2009). The range for Manning's roughness coefficient (n) were selected based on values for clean, straight reaches to very weedy reaches (Chow, 1959). The initial range for the flood wave coefficient (k_s) was selected based on the maximum theoretical range identified in Jain (2001). The initial ranges for friction factors (f_c, f_s) were selected based on the range of friction factors appearing on the Moody Diagram (Moody, 1944). The value for conduit tortuosity (τ_c) was assumed to be within the ranges of conduit tortuosity reported for looping cave systems and water-table cave systems by Jouves et al. (2017). Ranges for both the fracture lateral distance adjustment factor (dx_f) and the matrix lateral distance adjustment factor (dx_m) were assumed to have a maximum value of one, corresponding to the centroid-based distance for each groundwater cell, and a low value corresponding to a lateral distance approximately equal to the height of the groundwater table. Initial ranges for conduit and swallet diameters (D_c and D_S respectively) were based on measurements reported in Husic et al. (2017a) and Puckett (2015). The range of perched-fracture flow threshold ($h_{pa\ th}$) was specified from a low value to a maximum depth of bedrock above the aquitard.

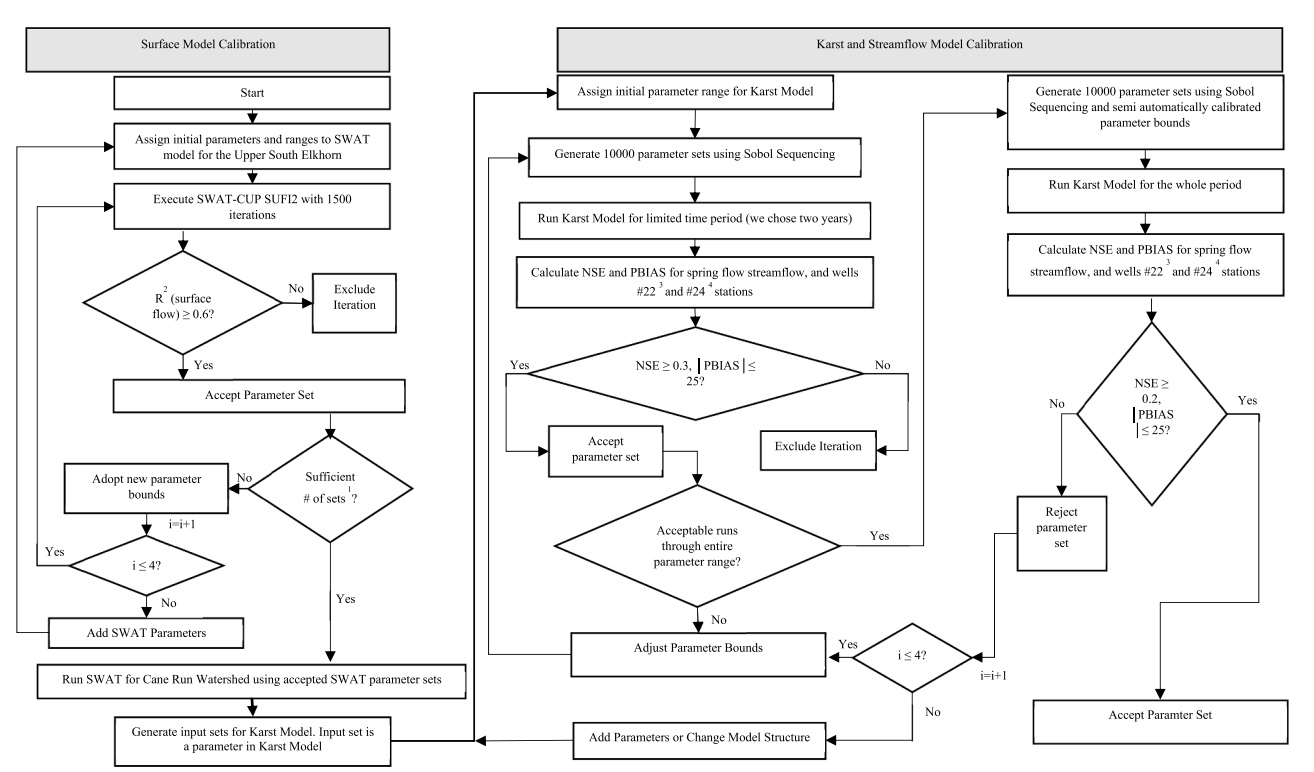
We tested the aquitard's sensitivity using different low hydraulic conductivities for the aquitard, however, this had no impact on the results. Therefore, the aquitard is treated as impermeable. The three dimensional fracture network crosses through the aquitard; therefore the perched aquifer at the lower portion of the vadose zone only drains through the fracture network when an aquitard member is present. This model parameterization was based on the concept that the fractures in the bedrock extend through limestone members formed with high clay or silt content, but diffuse flow through the surrounding rock matrix is

3.4. Model simulations

Model simulations were performed using MATLAB R2017a on an institutionally shared high-performance computing cluster with 9000 processor cores, 35 TB of RAM, and 1.3 PB of high-speed disk storage. Preparation of geospatial inputs, pre-processing, and post-processing of results was performed using ArcMap 10.4.1, ArcSWAT 2012 version 10.4.19, SWAT-CUP version 5.1.6.2, and MATLAB R2017a on a PC with Intel Xeon CPU of two logical processors with 3.60 GHz and RAM of

Table 3 Initial, final, and accepted fluviokarst model parameter ranges.

#	Parameter Name	Symbol	Initial range	e	Final range		Accepted range			Units	Reference/Justification	
			Min	Max	Min	Max	Min Max		Accepted			
1	Matrix Porosity	n_m	1x10 ⁻³	2	0.76	2.61	1.00 1.91		1.45	%	Williams, 2008	
2	Saturated Hydraulic Conductivity	K_s	1x10 ⁻⁹	5x10 ⁻⁶	1.5x10 ⁻⁶	6.1x10 ⁻⁶	1.98x10 ⁻⁶	5.83x10 ⁻⁶	5.41x10 ⁻⁶	${\rm m}~{\rm s}^{-1}$	Domenico and Schwartz, 1990	
3	Epikarst Porosity	n_{ep}	2	30	13	35	14	33	14	%	Klimchouk, 2004; Williams, 2008	
4	Epikasrt-Fracture Threshold Height	h_{epth}	0.01	1	0.01	0.92	0.43	0.80	0.80	m	Zhu et al. (2011)	
5	Pump Rate	Q_{pump}	5x10 ⁻⁶	0.01	8.61 x10 ⁻⁴	9.26 x10 ⁻³	8.39x10 ⁻³	8.98x10 ⁻³	8.94x10 ⁻³	m^3 s^{-1}	Carey and Stickney, 2005	
6	SWAT Run	SWAT	1	25	11	25	14	23	14	-	25 of Accepted SWAT	
7	Fracture Density	N	0.01	5	0.02	0.06	0.02	0.04	0.02	m^{-1}	Klimchouk, 2004	
8	Manning's n	n	0.025	0.15	0.06	0.15	0.07	0.12	0.12	$m^{1/6}$	Chow 1959	
9	Fracture Aperture	b	0.001	0.05	0.01	0.04	0.01	0.04	0.01	m	Worthington and Ford, 2009	
10	Flood Wave Coefficient	k_s	0	0.6	0.03	0.48	0.07	0.44	0.32	-	Jain, 2001	
11	Conduit Friction Factor	f_c	0.01	0.1	0.02	0.09	0.06	0.09	0.06	-	Moody, 1944	
12	Swallet Friction Factor	f_s	1.0*	3.0*	1.58*	3.18*	1.72*	2.59*	0.11	-	Moody, 1944	
13	Conduit Tortuosity	$ au_c$	1.1	1.3	1.16	1.31	1.17	1.30	1.22	m/m	Jouves et al. (2017)	
14	Swallet Tortuosity	$ au_s$	1.3	2.5	0.67	2.04	0.84	1.14	0.91	m/m	Jouves et al. (2017)	
15	Fracture Lateral Distance Adjustment	dx_f	0.05	1	0.01	0.87	0.04	0.86	0.50	-	Geometry considerations	
16	Matrix Lateral Distance Adjustment	dx_m	0.01	1	0.01	0.80	0.02	0.70	0.03	-	Geometry considerations	
17	Conduit Diameter	D_c	1.27–1.37	2.86-3.09	1.5–1.62	2.2-2.38	1.59–1.72	1.78–1.92	1.59–1.72	m	Husic et al. (2017a), Husic et al. (2017b)	
18	Swallets Diameter	D_S	0.11-0.21	1.17-1.71	0.13-0.24	0.67 - 1.28	0.18 – 0.35	0.35-0.67	0.18 – 0.35	m	Puckett (2015)	
19 *	Perched-fracture flow threshold $Value*f_c$	h _{path}	1	5	3.45	6.53	3.68	6.27	6.27	m	Well stage data	



- Sufficient number of sets to perform uncertainty analysis and to create multiple sets of inputs to the karst model. Water depth above the perched aquifer is compared graphically to the observations of well data. Well #22 is a well that measure observations of water depth above the perched aquifer. Well #24 is a well that measures piezometer head in the conduit.

Fig. 6. Multi-objective calibration diagram.

64 0 GB

3.5. Model calibration, validation, sensitivity and uncertainty analyses

Fig. 6 details the calibration and validation procedure. Multiobjective calibration was carried out using four stations including (1) springflow at Royal Spring (USGS 03288110) adjusted for a raw water intake upstream of the weir, (2) streamflow stage data and a stagedischarge curve at the surface stream outlet (Husic et al., 2017a), (3) a monitoring well directly intersecting the primary conduit, and (4) a monitoring well intersecting a perched aquifer.

The steps of model calibration were to: (i) reduce the initial parameter space using an optimization algorithm and visual inspection of results; and (ii) find optimal parameter values that met objective criteria including traditional statistical measures and visual fit. Sobol sequencing was used to generate the parameter values for sets of 1000 model runs to refine parameter ranges (Saltelli et al., 2008), and the SUFI2 optimization algorithm and visual fit was used to adjust parameter ranges (Abbaspour et al., 2007). In stage 2, optimal parameter fit was found by generating 10,000 parameter sets using Sobol sequencing, and the refined parameter ranges from semi-manual calibration. The karst model ran for the time period from January 1, 2010 to May 1, 2019, using the first year of simulation as model spin-up, five years for calibration, and four years as validation. For simulations on a monthly time scale, Moriasi et al. (2007) recommends Nash Sutcliff Efficiency (NSE) > 0.5 and absolute Percent Bias |PBIAS| < 25 as acceptable performance criteria. Model simulations on higher resolution time scales (e. g., hourly) are known to have lower values of performance metrics when compared to performance of the model when data is aggregated for a lower resolution time scale (Engel et al., 2007; Moriasi et al., 2007). Therefore, model hourly runs with NSE \geq 0.2 and |PBIAS| \leq 25% for spring discharge and NSE \geq 0.2 and |PBIAS| \leq 25% for streamflow were considered acceptable. Also, the P factor and R factor were evaluated following the method of Abbaspour et al. (2007). The P factor is percentage of data bracketed by the 95% prediction uncertainty measured at 2.5 and 97.5 percentiles, and the R factor is the ratio of the average distance between the two percentiles divided by the standard deviation of corresponding observed variable.

Both global and local sensitivity were performed because literature suggests the importance of both approaches (Saltelli et al., 2008; Abbaspour et al., 2007; Ceriotti et al., 2018). For example, Ceriotti et al. (2018) showed joint application of local and global sensitivity analyses was needed to characterize the importance/ranking of model parameters and hence propagation of uncertainty in their subsurface water model. Further, in our work, the modelling platform was new and we needed to understand the relative role of each model input (Ceriotti et al., 2018), so local sensitivity helped provide justification of the linkages. Global sensitivity was measured using a multiple regression model. This was chosen based on the ease of performance and a lower number of model simulations required to calculate the sensitivity. The multiple regression model regresses the parameters values sampled by the Sobol sequences against the values of the objective functions. T-tests were used to identify the significance effect of each parameter on the objective function (Abbaspour et al., 2007). Model performance was assumed to be sensitive to parameters with a p-value less than 0.05. Local sensitivity was investigated to test the influence of the 19 parameters on simulating the four objectives, including spring flow, streamflow, and piezometer heads in the perched aquifer well and conduit well. The parameters were changed one-at-a-time on the bases of 25%, 75%, 150%, and 200% parameter values for the parameters found in the most optimal model run. The decision of influence versus non-influence was based on the percent bias metric and visual inspection of the results. The local sensitivity results were built using the observations from 10/01/2012 to 10/01/2013 only because we have all observations for the four stations for this period.

Model uncertainty as measured by evaluating the mean and standard

deviation of acceptable model runs for each time step. Additionally, the average distance of the 95% prediction uncertainty (95 PPU), was evaluated. The 95 PPU was constructed using the 2.5% and 97.5% quantiles of the simulated values across all acceptable model runs for each time-step (Abbaspour et al., 2007).

3.6. Model results

Model evaluation results showed the model's ability to simulate four calibration objectives including stream flow, spring discharge, the groundwater level for the perched aquifer, and the groundwater level for the deeper aquifer. Results showed the model in general performed well for these four objectives (see Fig. 7 and parameters in Table 3) when acceptable runs were included in the results, i.e., NS > 0.2 and absolute PBIAS <= 25% for the 4 stations for the model evaluation, from the 10,000 simulations in the final production run. When compared to literature, the model performance is good to very good. Objective function values from our hourly model runs are comparable to objective function values of daily streamflow models considered acceptable (Gassman et al., 2007). The objective functions for spring discharge for our best model run surpass the satisfactory values subjected by Moriasi et al. (2007), for models with a monthly time-step. Watershed scale models have significantly reduced performance measures when using a shorter-duration time step (Gassman et al., 2007; Moriasi et al., 2007), which further substantiates that the model performs well.

Uncertainty assessment also showed acceptable performance of the model (Fig. 7). The average thickness of the 95 PPU (P factor) was 0.27, 0.18, 0.62, and 0.41 for spring flow, streamflow, perched aguifer well, and conduit well respectively. According to Abbaspour et al. (2007), P factor of less than one is sufficient to decrease uncertainty, and the P factor values of the hourly timestep model satisfies this rule. The observed spring flow was contained by the 95 PPU (R factor) during 20%, 18%, 40%, and 20% of the model timesteps for the four stations. The values of the R factor are lower than what is recommended for models with a daily timestep (Abbaspour et al., 2007), and the reason is attributed to the hourly time step of the model applied here and the potentially the low-quality of some observations. The observed spring discharge at the Royal Springs Gage is downstream from where abstractions are made by the Georgetown Municipal Water and Wastewater Service. Spring discharge data was adjusted for these abstractions; however, some error still exists. The streamflow data recorded some biases that needed to be removed using visual assessment. Also, the well data were collected at one point in the groundwater cell, whereas a dense monitoring well network would be more desirable. Additionally, the recommendations made by Abbaspour et al. (2007) are for models with a daily timestep, and as previously mentioned, recommended levels should be lower for models with an hourly time-step.

Sensitivity analyses showed that 14 out of 19 model parameters were sensitive to at least one of the four calibration objectives (see Table 4). Water discharge at the spring was sensitive to four parameters for global sensitivity and 5 for local sensitivity. Nevertheless, piezometric head at the conduit well was sensitive to 12 parameters when considering both global and local sensitivity analysis. It is important to note the goodness of fit for the multiple regression in Table 4, where R² and R²-adj are within 5% of one another for each objective function. These two measures are superior for the conduit well, which make the results of sensitivity analysis in this station more reliable. Sensitivity analysis results also showed that the performance of simulated streamflow was sensitive to 10 of the 19 model parameters when considering global and local sensitivity analyses (Table 4). Sensitivity of fracture aperture, fracture density, saturated hydraulic conductivity, and matrix porosity on flow at the surface was not expected, and suggests the subsurface karst at least partially impacts flow in the creek. The perched aquifer piezometer height was sensitive to 7 out of the 19 parameters for global and local sensitivity analyses.

Soil water percolation and runoff simulated with the SWAT ensemble

(a)

10

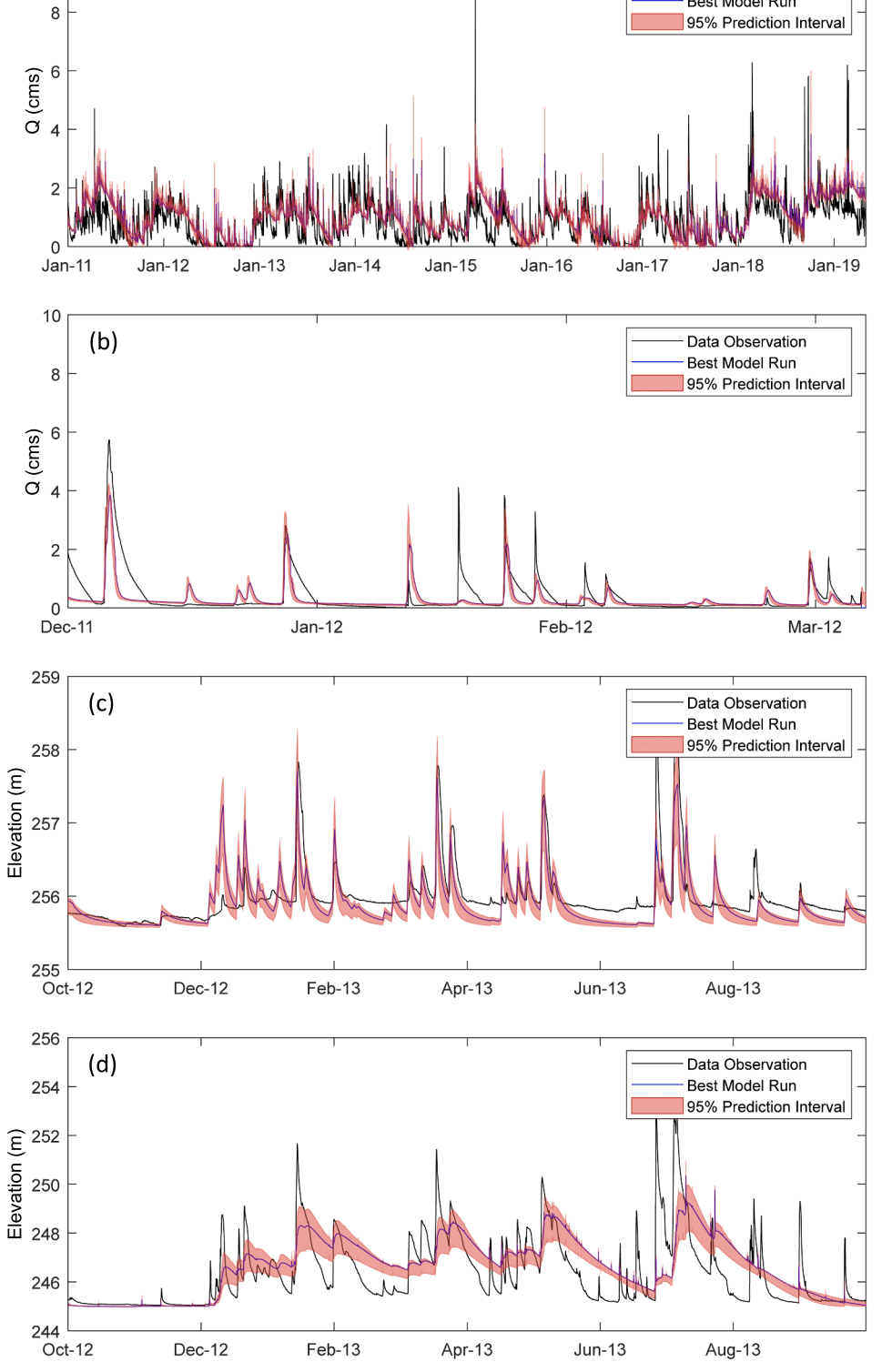


Fig. 7. Model evaluation results for multiple objective response variables. (a) Spring flow for entire period including best model run for calibration (NSE = 0.30, PBIAS = -0.14, R = 0.20, P = 0.27) and validation (NSE = 0.38, PBIAS = 0.01). (b) Surface stream flow (NSE = 0.55, PBIAS = 0.21, R = 0.18, P = 0.18). Well intersecting aquifer for upper groundwater model (NSE = 0.51, PBIAS = -0.24, R = 0.40, P = 0.62). Well intersecting the conduit (NSE = 0.35, PBIAS = -0.19, R = 0.20, P = 0.41).

Data Observation

Best Model Run

did not show sensitivity on the four response variables simulated with the fluviokarst model. The depth of water percolated from the soil to the sub-surface ranged by as much as -35% to +31% of the ensemble monthly mean during June for the 25 simulations; and the depth of water percolated annually ranged from -13% to +5% the ensemble annual mean. The runoff depth ranged from -6% to +25% the ensemble monthly mean during June for the 25 simulations; and runoff

depth ranged annually ranged from -11% to + 19% the ensemble annual mean. However, these ranges were not statistically significant for sensitivity of the surface and groundwater fluxes simulated. The reason is attributed to the pre-calibration carried out for SWAT so that runoff and soil transfer parameters were consistent with acceptable model runs reported for this region (Al Aamery et al., 2016, 2018).

Ensemble-average pathway results for the 9 years of simulation

Journal of Hydrology 593 (2021) 125844

Table 4Sensitivity analysis results for karst parameters when considering multiple objectives.

# Pa	Parameter Name	Parameter	Q spring Global Sensitivity R ²	Q surface Perched aq. we			ed aq. well	. well Conduit well						Total	
				0.33	Local Global Sensitivity Influence? R ² R ² -adj p-value	Sensitivity	0.34	Local Sensitivity	Global Sensitivity		Local Sensitivity	Global Sensitivity		Local Sensitivity	Sensitivity
								Influence?	nfluence? R ²	0.2	Influence?	R^2 0.6	0.62	Influence?	=
			R ² -adj	0.32		0.33	0.33	R ² -adj 0.1	0.18		R ² -adj 0	0.61			
			p-value			p-value			p- value			p- value			
1	Matrix Porosity	n_m	0		No	0		No	0.4		Yes	0.35		No	Yes
2	Saturated Hydraulic Conductivity	K_s	0		Yes	0		Yes	0		Yes	0		Yes	Yes
3	Epikarst Porosity	n_{ep}	0.36		No	0.17		No	0.38		No	0.4		No	No
4	Epikasrt-Fracture Threshold Height	ep_{th}	0.37		No	0.25		No	0.35		No	0.39		No	No
5	Pump Rate	Q_{pump}	0.38		No	0.33		No	0.22		No	0.39		Yes	Yes
6	SWAT Run	SWAT	0.21		No	0.39		No	0.39		No	0.31		No	No
7	Fracture Density	N	0.36		No	0		No	0		Yes	0		Yes	Yes
8	Manning's n	n	0.38		No	0		No	0.36		Yes	0.1		Yes	Yes
9	Fracture Aperture	b	0.31		Yes	0		Yes	0.4		Yes	0.27		Yes	Yes
10	Flood Wave Coefficient	k_s	0.3		No	0.06		No	0.31		No	0.01		No	Yes
11	Conduit Friction Factor	f_c	0.01		Yes	0.2		Yes	0.38		No	0		Yes	Yes
12	Swallet Friction Factor	f_s	0.37		No	0.39		No	0.4		No	0.34		No	No
13	Conduit Tortuosity	$ au_c$	0.35		Yes	0.38		Yes	0.21		No	0.28		Yes	Yes
14	Swallet Tortuosity	$ au_s$	0.4		No	0		Yes	0.35		Yes	0.37		Yes	Yes
15	Fracture Lateral Distance Adjustment	dx_f	0.4		No	0.4		No	0.25		No	0.03		No	Yes
16	Matrix Lateral Distance Adjustment	dx_m	0.33		No	0.26		No	0.32		No	0.39		No	No
17	Conduit Diameter	D_c	0		Yes	0		Yes	0.39		No	0		Yes	Yes
18	Swallets Diameter	D_S	0.15		No	0		Yes	0.39		No	0.05		Yes	Yes
19	Perched-Fracture flow threshold	h _{path}	0.39		No	0.4		No	0		Yes	0.4		No	Yes

Gray shaded cells represent sensitive parameters.

suggest that, while both karst and fluvial pathways are important, Royal Spring exports most of the water (63%) from the coupled surface-subsurface system whereas the surface stream outlet drains less (26%). The remaining water balance (11%) is pumped from the aquifer for human consumption or agricultural uses. Water exiting at Royal Spring consists of drainage transported by the fracture-conduit network. Annual average sources of water to the fracture-conduit network are dominated by recharge from soil, vadose zone and perched aquifers (70%) with lesser amounts from previously recharged water stored in the rock matrix (18%), landscape sinkholes (9%), and in-stream swallets

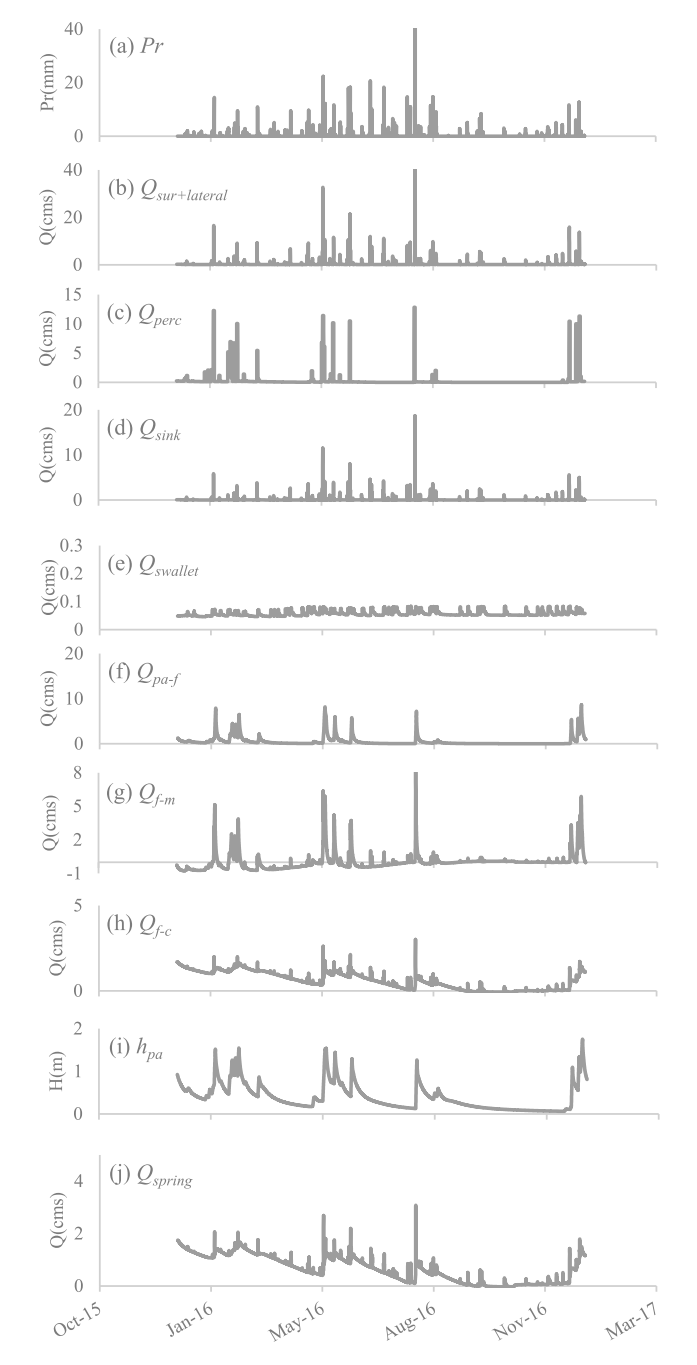


Fig. 8. Modeled hydrologic pathways for the fluviokarst basin for 2016 calendar year, including (a) precipitation, Pr, (b) discharge from runoff and soil lateral flow, *Qsur* + *lateral*, (c) soil water percolation recharge, *Qperc*, (d) sinkhole recharge, *Qsink*, (e) swallet recharge, *Qswallet*, (f) perched aquifer to fracture network discharge, *Qpa-f*, (g) fracture network to rock matrix discharge, *Qf-m*, (h) fracture network to conduit discharge, *Qf-c*, (i) perched aquifer potentiomeric surface, *hpa*, (j) springflow discharge, *Qspring*.

(3%). Water at the surface watershed outlet is dominated by runoff overflow during events.

Time series results of hydrologic pathways (see Fig. 8) show how each pathway imprints on the net shape of the spring and stream hydrographs but at different timescales. Storm pulses and slower percolation of water from the near surface aquifer are easily observed to imprint the hydrograph results in Fig. 8. Storm pulses cause daily fluctuations of fracture flowrate and spring flowrate time series reflecting delivery from the swallet and sinkhole features. Slower percolation cause weekly to monthly time series structure of fracture flowrate and spring flowrate reflecting delivery from soil percolation, vadose zone and perched aquifers (Fig. 8). The slowest contributor to the time series structure is the rock matrix. The rock matrix is shown to fill during storm events and wet periods via the fracture network and soil percolation. This is seen in time series results as Q_{f-m} is positive during storm events in Fig. 8g. The rock matrix then drains and discharges to the fracture network during dry periods, as is shown in Fig. 8g when Q_{f-m} is negative during dry periods.

Imprint of individual pathways also reflects their residence time. Residence times in karst pathways vary by five orders of magnitude (Table 5), ranging from less than one hour in vertical swallets, 12.7 h in longitudinal conduits, 12.7 days in the vadose zone and epikarst, and 142.7 days in the bedrock matrix. Time series of the fracture-conduit flow and springflow are identical, highlighting the well-defined fracture-conduit network that dominates spring discharge.

4. Discussion

4.1. Multi-objective calibration and model advantages and disadvantages:

Our model evaluation results suggest the need for multi-objective calibration for the fluviokarst numerical model developed in this study. Using the model formulated and applied here, we suggest including calibration of streamflow, springflow, and potentiometric surfaces of perched and deep aquifers. Sensitivity analyses of the model showed cumulatively 14 out of 19 model parameters were sensitive during calibration (Table 4). The sensitivity results offer confidence the acceptable model runs were providing a reasonable depiction of the subsurface rock structure and water pathways. However, using just one objective in calibration likely is insufficient. For example, global sensitivity analyses showed only 4 out of 19 parameters were sensitive when only springflow at Royal Spring was considered. If the model was calibrated only with springflow, the resultant parameterization may be sufficient for estimating springflow; however the underlying aquifer structure and its pathways would be questionable.

Review of the literature shows karst models sometimes use multiple model responses during calibration, such as springflow and potentiometric surface via well stage (Pétré et al., 2019), while more often karst studies only use one response during calibration, such as only springflow or only groundwater level (Candela et al., 2009; Tritz et al., 2011; Ali et al., 2012; Doummar et al., 2018; Ou et al., 2018). Few karst or fluviokarst studies, to our knowledge, use surface water flows, springflows and potentiometric surfaces in calibration and highlighting this importance for fluviokarst is one contribution of this paper. Recommendations for karst modelling previously suggested multi-objective calibration using water chemistry and water isotopes (Hartmann et al., 2014). Our

Table 5Mean residence times for fluviokarst features.

Feature	Annual mean
Swallet	4.2 mins
Conduit	12.7 hrs
Fractures	21.6 hrs
Matrix	142.7 days
Vadose zone, perched Aquifer	11.8 days

results extend this multi-objective recommendation to surface and subsurface stage and discharge when information about fluviokarst pathways and aquifer structure are sought after.

One advantage of the fluviokarst model is its capability to simulate connectivity between surface stream hydraulics and cave hydraulics *via* the in-stream swallets. Results suggest the model's utility for future fluviokarst basins when pathways connectivity is sought after. The numerical structure and its optimization simultaneously simulate surface stream hydraulics, unsaturated flow, cave hydraulics, and the connectivity between the surface and subsurface via the in-stream swallets. The benefit is the model outputs the potentiometric surface of perched and deep aquifers and flow results at the spring, the stream, and flowrates for the connected features. These results for both water discharge and the potentiometric surface will be useful for applications of the model to predict downstream water delivery and water storage.

A second advantage of the model was our ability to omit prior biases of how the system might be behaving. A priori we anticipated reasonable contributions to the spring hydrograph from sinking streams, the fracture network, and the saturated rock matrix as well as the behavior of swallets to pirate surface streamflow to the subsurface conduit. Our prior biases were based on previous karst literature that tends to emphasize the three end-member concept in a number of papers (e.g., Pinault et al., 2001; White, 2002; Worthington, 2007; Long, 2009) and the optical nature of the swallets as sinks during our field reconnaissance. Nevertheless, we recognized the potential for the fracture network or rock matrix to dominate subsurface flows, as detailed in some papers (Matthäi and Belayneh, 2004), and the potential for flow reversal of fluviokarst features (Chen and Goldscheider, 2014; Hensley et al., 2014), including one named estavelle in our system (Thrailkill et al., 1991). Therefore, we used a wide range of prior parameterization to consider all potential storage zones and transfers contribution to karst transfer phenomena. Optimization of the model structure allowed an unbiased parameterization of the 20 + pathways by using the multiple objective functions and Sobol sequences. The lack of bias in compartments is reflected in the spring water residence time that is deconvoluted across five orders of magnitude (Table 5).

One disadvantage was the numerical model's computational expense. Simulation time for production runs was approximately 168 h on the computer cluster using 1,000 cores with 4 TB RAM. This has a monetary expense of approximately \$15 k USD. The computational cost was high due to simultaneously solving the system of non-linear equations for the lower groundwater model via the trust-region with dogleg method with 1,000 numerical iterations per model time step (see methods section, Dennis and Schnabel, 1996). We tested other numerical techniques, including line search optimization, but we found no decrease in computation time and less accuracy. Future research might investigate further programing efficiency of our code, but nevertheless computational costs will continue to be a disadvantage for process-based models of fluviokarst systems.

Another disadvantage was the numerical model's cost for input data. In the model application, the streams and karst conduit were well-characterized from previous tracer tests, lidar mapping, electrical resistivity mapping, well data collection, isotope tracer studies, data-driven water budgets, and routine long term and event-based water quality measurements. This prior information made setup of the model domain feasible; however, this vast array of data may not be available for other fluviokarst study sites.

4.2. Investigate fluviokarst aquifer structure, pathways, and in-stream swallets:

Modelling results of aquifer structure suggest classification of the basin as relatively mature fluviokarst with defining features that include in-stream swallet features, a well-defined fracture-conduit network, and a shallow, phreatic primary cave. These features add to discussion of karst morphology and its hydrologic behavior in the context of features

mentioned by others (Drysdale et al., 2001; White, 2002; Massei et al., 2003; Phillips and Walls, 2004; Herman et al., 2008; Husic et al., 2017a, 2017b). The in-stream swallet features provide connectivity between surface stream and subsurface flow, and these features together with the presence of both a fluvial network and karst network demonstrate the 'fluviokarst' classification (Phillips and Walls, 2004). The well-defined fracture-conduit network is evidenced by the high fracture-matrix permeability ratio (10⁵ to 10⁸) from model optimization, which places the system in the regime of fracture flow being important for subsurface karst drainage (Matthäi and Belayneh, 2004). This leads to a classification of the system as a 'mature' karst aquifer with pronounced dissolution and multiple levels of porosity including turbulent conduit flow, fracture flow, and Darcian flow (White, 1999; Hartmann et al., 2013). The karst spring is supplied by a primary phreatic conduit, and characteristics of phreatic systems are adverse subsurface gradients controlling cave hydraulics and springflow (Drysdale et al., 2001; White, 2002; Massei et al., 2003; Herman et al., 2008; Husic et al., 2017a).

The dominant hydrologic pathways in the fluviokarst basin show analogy with groundwater flow in many karst basins more generally, with some modification. Fig. 9 shows the springflow together with (i) swallets and sinkhole flowrates entering the fracture-conduit network from the surface, (ii) soil, epikarst and perched aquifer water entering from the upper groundwater model, and (iii) rock matrix flowrate entering from the lower groundwater model. These three flowrates in Fig. 9 are analogous to triunal-transfer, including quick-, intermediate-, and slow-flow, mentioned in karst studies (e.g., Pinault et al., 2001; Worthington, 2007; Long, 2009). The pressure response of these three flowrates are felt immediately at the spring because the fracture-conduit network is mature and the conduit is phreatic. The activation and deactivation of pathways to the fracture-conduit network shifts the pressure response and changes the shape of the spring hydrograph, including inflections or sharp change in the recession gradient. The pressure response of this fluviokarst aquifer is corroborated by other karst studies such the concept of stored water being pressed out of conduits on the rising limb of the hydrograph (e.g., Hartmann et al., 2014) and the piston effect during extreme events (e.g., Lastennet and Mudry, 1997; Milanović, 2014). We point out the pressure response is immediately felt at the karst spring in Fig. 9, although the arrival of quick-flow from swallets and sinkholes does not occur until later. For example, average transit time through fractures and conduits is approximately 22 and 13 h, respectively (see Table 5).

The pressure response of mature and phreatic fracture-conduit networks suggests some modification when interpreting hydrologic pathways impact on springflow in fluviokarst basins similar to those in this study. Our modelling evidence supports the spring hydrograph as a four component sources including a pressure response exporting previously stored water, arrival of underground runoff at the spring, arrival of percolated soil and epikarst water at the spring, and arrival of rock matrix water at the spring. The arrival of these components is disconnected in time from springflow inflections because the system is phreatic. Hydrologists often interpret spring hydrograph inflections to indicate shifts in the origin of water from aquifer zones with differing porosity, transfer and storage characteristics (Talarovich and Krothe, 1998; Baedke and Krothe, 2001; Pinault et al., 2001; Worthington, 2007; Fiorillo, 2011; Hosseini et al., 2017; Xu et al., 2016). For example, inflections in recession curves are reported to reflect a shift from runoff in the caves to water draining fractures to water draining rock matrix (Fiorillo, 2014; Xu et al., 2016). Scientists might consider modifying this interpretation by considering potential for disconnect between the pressure response and arrival of different source waters.

In-stream swallets directly connect the surface stream network to the karst aquifer, and the role of these features is unique to fluviokarst. Our modelling results suggest the in-stream swallets only pirate flow from the surface stream to the karst subsurface, and flow reversal does not occur for this system. The overall impact of the in-stream swallets was rather small, and the in-stream swallets are responsible for just 3% of

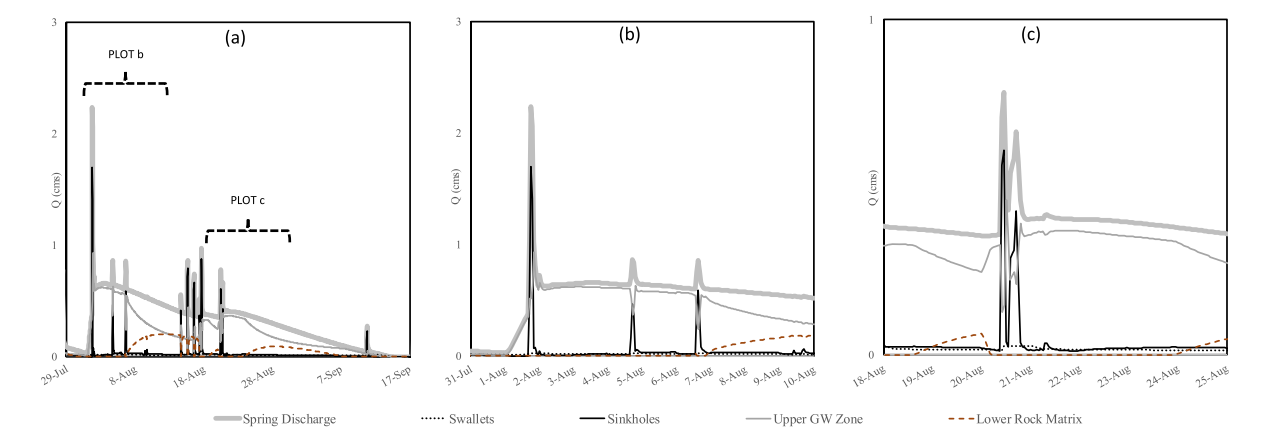


Fig. 9. Contributions of swallets, sinkholes the upper groundwater zone and lower rock matrix during an event, and the pressure response experienced at the primary spring.

water arriving at the primary spring. The net influence is owed to the relatively small diameter of the in-stream swallets and the average swallet diameter was just 26 cm. For fluviokarst, we define here a vertical to longitudinal conveyance ratio, C_R , to describe the conveyance of water through the vertical swallets relative to the longitudinal conduits. We define a dimensionless conveyance ratio as

$$C_R = \frac{\sum_{i=1}^n D_{S-i}^2}{\sum_{i=1}^m D_{C-j}^2} \tag{15}$$

where the diameters of n swallets and m conduits can be considered for the fluviokarst system. C_R equaled 0.3 for our optimal model run highlighting the small influence of swallet vertical conveyance relative to the conduit longitudinal conveyance for this system.

As further discussion, we used our numerical model to investigate how changes in the conveyance ratio impacts contributions of the instream swallets to springflow. We set up hypothetical model simulations where swallet diameters and conduit diameters were varied to study the influence of the conveyance ratio on in-stream swallet contribution to springflow. Swallet diameter was varied from 13 cm to 104 cm, and conduit diameter was varied from 83 cm to 330 cm. Results

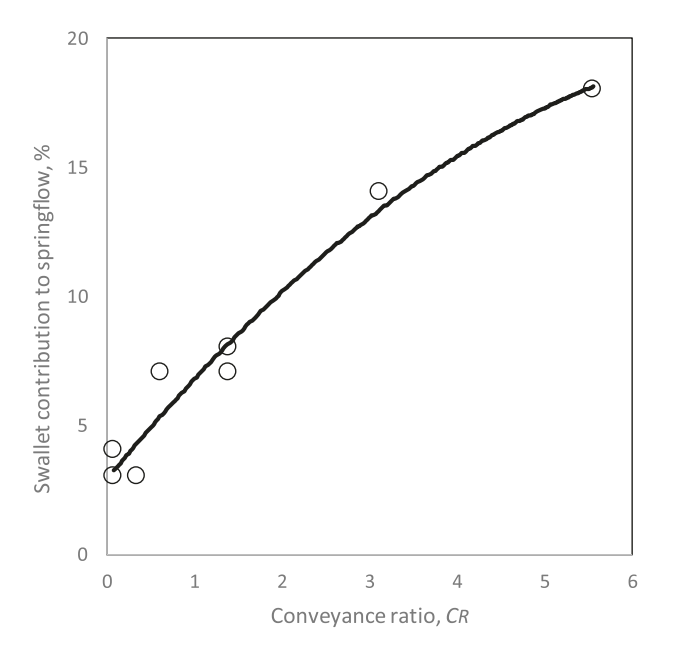


Fig. 10. Swallet contribution to springflow as a function of the conveyance ratio.

in Fig. 10 show changes to the conveyance ratio shifts contributions of in-stream swallets to the total annual springflow by nearly an order of magnitude. We qualify that the exact numbers for percent contribution of swallets to springflow found in Fig. 10 is an artifact of the specific features of the study site and the model's parameterization. Nevertheless, the order of magnitude influence of the conveyance ratio on instream swallet contributions should be highlighted for fluviokarst. Swallet diameters and conduit diameters are extremely difficult to measure in the field, especially for networks of swallets and phreatic conduits. Despite our field efforts, the diameters were kept as parameters given our uncertainty surrounding the variables. We point out the importance of estimating and parameterizing swallet and conduit diameters for investigating fluviokarst basins. Researchers might work towards improving methods for such estimates, and for example tomographic methods serve as one potential tool.

4.3. Discussion of model transferability and its alternatives to other karst basins:

The model formulated and applied in this study allows us to discuss our new karst model more broadly in the context of existing karst modelling alternatives. Thereafter, we discuss the applicability of transferring this model, and other karst model alternatives, to karst study sites with varying degrees of information.

As a brief review to provide context, karst models are classified as distributed models, reservoir models, or hybrids of the two (Hartmann et al., 2014; Knöll et al., 2020; Ollivier et al., 2020). Distributed models refer to process-based modelling where the domain is divided to groundwater cells and the governing equations are solved for flow in one or more directions using numerical methods (e.g., Doummar et al., 2012; Chang et al., 2015; Qiu et al., 2019; Kavousi et al., 2020). Reservoir models refer to storage-discharge equations where one or more linear or nonlinear transfer functions are applied to represent flow from the total basin or decomposed zones (i.e., quick-, intermediate-, slow-flow transfer zones, e.g., Husic et al., 2019b). Some authors refer to reservoir models as 'lumped models' (e.g., Hartmann et al., 2014), however we avoid this term because lumped is also used to indicate process-based models averaged across basins or sub-basins in hydrology (Singh, 2012).

Discrete elements have been added to both distributed and reservoir model structures. Including discrete elements suggests knowledge of the conduit network structure throughout the basin. More often discrete conduits are included in distributed structures (Chang et al., 2015; Qiu et al., 2019; Kavousi et al., 2020) although discrete conduit modelling can also be coupled within a reservoir structure for the broader groundwater basin (e.g., Husic et al., 2020).

The model formulated and applied here classifies as a combined discrete continuum (CDC) fluviokarst numerical model and shows some characteristics of existing karst models as well as unique modelling features. The model here is CDC fluviokarst because: the upper groundwater model divides the groundwater domain to sub-basins and then distributes each sub-basin vertically; the lower groundwater models solves the governing equations for discrete fractures, swallets and conduits; and the surface stream model simulates the fluvial system aboveground and interacts with karst swallets. Unique features include the numerical treatment of swallets, discrete elements for fractures, swallets and conduits, and coupling the timescales of water through the model. Simplified features are: the one-dimensional, vertical treatment of the upper groundwater model, and treating these sub-basins as three dimensionally distributed would be possible in future work; and global parameterization of hydraulic conductivity and rock porosity in the upper groundwater model, and further distributing these parameters could be possible if additional borings were collected throughout the groundwater basin.

The transferability of the model presented herein, as well as other karst distributed model and reservoir model alternatives, to karst study sites relies on the degree of information available and in turn leads to response variables of varying detail. The karst modeler is charged with representing the groundwater basin given the degree of geomorphologic data. The modeler can add a discrete network of conduits, fractures and their connectivity to the surface as subsurface data becomes available from well drillings, dye tracers and resistivity measurements. Without such data, specifying a discrete conduit network leads to increasing conjecture, and in turn increasing model complexity, and modelling results that are not defensible. For discussion purposes, we classify this information spectrum as known, or reasonably assumed, information about: (i) the primary springs only; (ii) springs and swallets; and (iii) springs, swallets, primary conduits and fractures.

Reservoir models without discrete elements provide a reasonable karst modelling choice when the known information for the basin is flow at the primary spring. Husic et al. (2019b) showed a four-reservoir model outperformed one-, two- and three-reservoir models when primary spring discharge was predicted. The multi-reservoir structure captured the flow signal reflective of multi-porosities believed or known to exist in the Husic et al. (2019b) study. Results were limited to residence time and time-distributed flowrates associated with each reservoir. Distributed model simulations without discrete elements are also possible in some cases when primary information is only available for the spring. However, multi-continuum distributed models will quickly lead to overparameterization unless at least some information is known about the matrix structure, and results of such distributed model results are viewed as theoretical (e.g., Hartmann et al., 2014). We suggest the fluviokarst model with its CDC structure, and other similarly formulated CDC models, are too complex when primary spring information only is the response available.

Reservoir or distributed models with discrete elements added are possible, albeit increasingly hypothetical, when known information exists for springs and swallets, such as primary springs, secondary springs, in-stream swallets and landscape sinkholes. Kavousi et al. (2020) used permutations of discrete conduit structures when only swallet and spring information were available, and applied model evaluation criteria to arrive at the most plausible discrete conduit structure. Additionally, the autocorrelation and cross-correlation structure of swallets and springs can be used to infer the conduit structure in karst systems (e.g., Massei et al., 2006), which in turn can lead to construction of discrete conduit-swallet networks. Nevertheless, results of conveyance rates and conduit dimensions become increasingly hypothetical for discrete conduit-swallet networks, unless swallet-spring datasets are spatially dense. We suggest the fluviokarst model herein, and similar CDC models, be viewed as hypothetical when applied when only swallet and spring datasets are available.

Discrete networks built-in to CDC models, such as the model

presented herein, become increasingly applicable to basins where information of conduits and fracture structure and responses variables as well as spring and swallet datasets are available. A known, or reasonably assumed, conduit-swallet network allows the modeler to construct a subsurface stream or pipe network at the onset. With a network defined, the modeler can discretize continuum using geologic information (e.g., presence of aquitards, changing rock type) using physical considerations similarly to watershed hydrology modelling. As shown here, multiple response variables from springs, surface flows and swallets, and wells in fracture-dominated and conduit drainages add leverage to parameterizing CDC models. In turn, conveyance results from different hydrologic pathways become increasingly believable. For these reasons, we suggest the model herein, and similar CDC models, are most applicable to karst basins with data available to define conduit-swallet networks as well as data from multiple locations and features to be used for model evaluation.

5. Conclusion

Our model evaluation results suggest the need for multi-objective calibration for fluviokarst numerical modelling. Using only a single response variable (i.e. springflow) resulted in model sensitivity to only 4 out of 19 model parameters. Multi-objective calibration with streamflow, springflow, and potentiometric surfaces of perched and deep aquifers showed sensitivity of 14 out of 19 model parameters, offering greater confidence the acceptable model runs depict the aquifer structure and hydrologic pathways.

Advantages of the fluviokarst model contributed herein are its capability to simulate connectivity between surface stream hydraulics and cave hydraulics *via* the in-stream swallet, and the model's ability to omit prior biases of how the system might be behaving. Disadvantages are the numerical model's cost for input data and the model's computational expense. Production runs required 168 h on the cluster using 1000 cores with 4 TB RAM.

Modelling results suggest classification of the basin as relatively mature fluviokarst with in-stream swallet features, a well-defined fracture-conduit network, and a shallow, phreatic primary cave. These features produce hydrologic pathways classified as triunal-transfer. However, the arrival of source waters is disconnected in time from the springflow response. The pressure response of mature and phreatic fracture-conduit networks suggests some modification when interpreting hydrologic pathways impact on springflow in fluviokarst basins similar to those in this study. Karst hydrologists might consider modifying their interpretation by considering a four component model that includes the disconnect between the pressure response and arrival of different source waters. The disconnect might be consider pathway residence time; and for example our results suggest pathways vary by five orders of magnitude, ranging from less than one hour in vertical swallets, 12.7 h in longitudinal conduits, 12.7 days in the vadose zone and epikarst, and 142.7 days in the bedrock matrix.

In-stream swallets directly connect the surface stream network to the karst aquifer, and the role of these features is unique to fluviokarst. We define a dimensionless vertical to longitudinal conveyance ratio, and investigation shows the ratio helps predict swallet behavior. An order of magnitude influence of the conveyance ratio on in-stream swallet contributions is found for this fluviokarst basin. Given the sensitivity of the conveyance ratio, we suggest advancement is needed for measuring swallet and conduit diameters.

CRediT authorship contribution statement

Nabil Al Aamery: Methodology, Software, Validation, Formal analysis, Writing - original draft, Visualization. Ethan Adams: Conceptualization, Methodology, Software, Data curation, Writing - original draft. James Fox: Conceptualization, Methodology, Investigation, Resources, Writing - original draft, Supervision, Project

N. Al Aamery et al. Journal of Hydrology 593 (2021) 125844

administration, Funding acquisition. Admin Husic: Conceptualization, Methodology, Software. Junfeng Zhu: Conceptualization, Investigation, Resources. Morgan Gerlitz: Investigation, Data curation. Carmen Agouridis: Investigation, Resources. Leonie Bettel: Investigation, Data curation.

Declaration of Competing Interest

The authors declare that they have no known competing financial interests or personal relationships that could have appeared to influence the work reported in this paper.

Acknowledgements

We gratefully acknowledge the financial support of this research from the Kentucky Senate Bill 271B Water Quality program and National Science Foundation Awards #1632888 and #1933779. We gratefully acknowledge the Center for Computational Sciences at the University of Kentucky for the support provided during model executions on the supercomputer. We acknowledge the work of Jim Currens and Chuck Taylor in setting up and maintaining the groundwater monitoring network. The thank the comments of three anonymous reviewers and Editor Corradini, and addressing these comments greatly improved the paper.

Appendix A. Supplementary data

Supplementary data to this article can be found online at https://doi.org/10.1016/j.jhydrol.2020.125844.

References

- Abbaspour, K.C., Yang, J., Maximov, I., Siber, R., Bogner, K., Mieleitner, J., Zobrist, J., Srinivasan, R., 2007. Modelling hydrology and water quality in the pre-alpine/alpine Thur watershed using SWAT. J. Hydrol. 333 (2–4), 413–430.
- Al Aamery, N., Fox, J.F., Snyder, M., 2016. Evaluation of climate modeling factors impacting the variance of streamflow. J. Hydrol. 542, 125–142.
- Al Aamery, N., Fox, J.F., Snyder, M., Chandramouli, C.V., 2018. Variance analysis of forecasted streamflow maxima in a wet temperate climate. J. Hydrol. 560, 364–381.
- Ali, R., McFarlane, D., Varma, S., Dawes, W., Emelyanova, I., Hodgson, G., Charles, S., 2012. Potential climate change impacts on groundwater resources of south-western Australia. J. Hydrol. 475, 456–472.
- Baedke, S.J., Krothe, N.C., 2001. Derivation of effective hydraulic parameters of a karst aquifer from discharge hydrograph analysis. Water Resour. Res. 37 (1), 13–19.
- Bandy, A.M., Cook, K., Fryar, A.E., Zhu, J., 2019. Differential transport of Escherichia coli isolates compared to abiotic tracers in a karst aquifer. Groundwater.
- Bear, J., Tsang, C.F., De Marsily, G., 2012. Flow and contaminant transport in fractured rock. Academic Press.
- Brooks, R.H., Corey, A.T., 1964. Hydraulic properties of porous media. Hydrology papers (Colorado State University) no. 3.
- Candela, L., von Igel, W., Elorza, F.J., Aronica, G., 2009. Impact assessment of combined climate and management scenarios on groundwater resources and associated wetland (Majorca, Spain). J. Hydrol. 376 (3–4), 510–527.
- Carey, D.I., Stickney, J.F., 2005. Groundwater resources of Hancock County. Kentucky. Kentucky Geological Survey, ser. 12. County Report 46.
- Ceriotti, G., Guadagnini, L., Porta, G., Guadagnini, A., 2018. Local and global sensitivity analysis of Cr (VI) geogenic leakage under uncertain environmental conditions. Water Resour. Res. 54, 5785–5802. https://doi.org/10.1029/2018WR022857.
- Chang, Y., Wu, J., Liu, L., 2015. Effects of the conduit network on the spring hydrograph of the karst aquifer. J. Hydrol. 527, 517–530.
- Chang, Y., Wu, J., Jiang, G., Zhao, X., Zhang, Q., 2019. Investigating the appropriate model structure for simulation of a karst catchment from the aspect of spatial complexity. Environ. Earth Sci. 78 (1), 13.
- Chen, Z., Goldscheider, N., 2014. Modeling spatially and temporally varied hydraulic behavior of a folded karst system with dominant conduit drainage at catchment scale, Hochifen-Gottesacker, Alps. J. Hydrol. 514, 41–52.
- Chow, V., 1959. Open-channel hydraulics, Vol. 1. McGraw-Hill, New York.
- Cressman, E.R., Peterson, W.L., 1986. Ordovician system. The geology of Kentucky: a text to accompany the geologic map of Kentucky. U.S. Geol. Surv. Prof. Pap.
- Cressman, E.R., 1967. Geologic map of the Georgetown quadrangle, Scott and Fayette counties. Kentucky No. 605.
- Currens, J.C., Taylor, C.J., Webb, S., Zhu, J., Workman, S., Agouridis, C., Husic, A., 2015. Initial Findings from the Karst Water Instrumentation System Station, Royal Spring Groundwater Basin, Kentucky Horse Park 2010–2014. In: In Proceedings Kentucky Water Resources Annual Symposium, Kentucky Water Resources Research Institute, pp. 9–10.

- Dennis Jr, J.E., Schnabel, R.B., 1996. Numerical methods for unconstrained optimization and nonlinear equations Vol. 16, Siam.
- Domenico, P.A., Schwartz, F.W., 1990. Physical and chemical hydrogeology. Domenico, P.A., Schwartz, F.W., 1998. Physical and chemical hydrogeology. Vol.
- Domenico, P.A., Schwartz, F.W., 1998. Physical and chemical hydrogeology, Vol. 506. Wiley, New York.
- Doummar, J., Sauter, M., Geyer, T., 2012. Simulation of flow processes in a large scale karst system with an integrated catchment model (Mike She)–Identification of relevant parameters influencing spring discharge. J. Hydrol. 426, 112–123.
- Doummar, J., Kassem, A.H., Gurdak, J.J., 2018. Impact of historic and future climate on spring recharge and discharge based on an integrated numerical modelling approach: Application on a snow-governed semi-arid karst catchment area. J. Hydrol. 565, 636–649.
- Drahovzal, J.A., Harris, D.C., Wickstrom, L.H., Walker, D., Baranoski, M.T., Keith, B., Furer, L.C., 1992. The East Continent Rift Basin: A New Discovery. Special Publication, Kentucky Geological Survey, p. 18.
- Drysdale, R., Pierotti, L., Piccini, L., Baldacci, F., 2001. Suspended sediments in karst spring waters near Massa (Tuscany), Italy. Environ. Geol. 40 (8), 1037–1050.
- Engel, B., Storm, D., White, M., Arnold, J., Arabi, M., 2007. A Hydrologic/Water Quality Model Applicatil 1. JAWRA J. Am. Water Resourc. Assoc. 43 (5), 1223–1236.
- Fiorillo, F., 2011. Tank-reservoir drainage as a simulation of the recession limb of karst spring hydrographs. Hydrogeol. J. 19 (5), 1009–1019.
- Fiorillo, F., 2014. The recession of spring hydrographs, focused on karst aquifers. Water Resour. Manage. 28 (7), 1781–1805.
- Gassman, P.W., Reyes, M.R., Green, C.H., Arnold, J.G., 2007. The soil and water assessment tool: historical development, applications, and future research directions. Trans. ASABE 50 (4), 1211–1250.
- Gupta, R.S., 2008. Hydrology and hydraulic systems. Waveland Press.
- Gupta, R.S., 2016. Hydrology and hydraulic systems. Waveland Press.
- Hartmann, A., Goldscheider, N., Wagener, T., Lange, J., Weiler, M., 2014. Karst water resources in a changing world: Review of hydrological modeling approaches. Rev. Geophys. 52 (3), 218–242.
- Hartmann, A., Weiler, M., Wagener, T., Lange, J., Kralik, M., Humer, F., Mizyed, M., Rimmer, A., Barbera, J.A., Andreo, B., Butscher, C., Huggenberger, P., 2013. Processbased karst modelling to relate hydrodynamic and hydrochemical characteristics to system properties. Hydrol. Earth Syst. Sci. 17 (8), 3305–3321.
- Hensley, R.T., Cohen, M.J., Korhnak, L.V., 2014. Inferring nitrogen removal in large rivers from high-resolution longitudinal profiling. Limnol. Oceanogr. 59 (4), 1152–1170.
- Herman, E.K., Toran, L., White, W.B., 2008. Threshold events in spring discharge: evidence from sediment and continuous water level measurement. J. Hydrol. 351 (1–2), 98–106.
- Hosseini, S.M., Ataie-Ashtiani, B., Simmons, C.T., 2017. Spring hydrograph simulation of karstic aquifers: Impacts of variable recharge area, intermediate storage and memory effects. J. Hydrol. 552, 225–240.
- Husic, A., Fox, J., Agouridis, C., Currens, J., Ford, W., Taylor, C., 2017a. Sediment carbon fate in phreatic karst (Part 1): Conceptual model development. J. Hydrol. 549, 179–193.
- Husic, A., Fox, J., Ford, W., Agouridis, C., Currens, J., Taylor, C., 2017b. Sediment carbon fate in phreatic karst (Part 2): Numerical model development and application. J. Hydrol. 549, 208–219.
- Husic, A., Fox, J., Adams, E., Backus, J., Pollock, E., Ford, W., Agouridis, C., 2019a. Inland impacts of atmospheric river and tropical cyclone extremes on nitrate transport and stable isotope measurements. Environ. Earth Sci. 78 (1), 36.
- Husic, A., Fox, J., Adams, E., Ford, W., Agouridis, C., Currens, J., Backus, J., 2019b. Nitrate pathways, processes, and timing in an agricultural karst system: Development and application of a numerical model. Water Resour. Res. 55 (3), 2079–2103.
- Husic, A., Fox, J., Adams, E., Pollock, E., Ford, W., Agouridis, C., Backus, J., 2020.Quantification of nitrate fate in a karst conduit using stable isotopes and numerical modeling. Water Res. 170, 115348.
- Jain, S.C., 2001. Open-channel flow. John Wiley & Sons.
- Jeannin, P.Y., 2001. Modeling flow in phreatic and epiphreatic karst conduits in the Hölloch cave (Muotatal, Switzerland). Water Resour. Res. 37 (2), 191–200.
- Jouves, J., Viseur, S., Arfib, B., Baudement, C., Camus, H., Collon, P., Guglielmi, Y., 2017. Speleogenesis, geometry, and topology of caves: A quantitative study of 3D karst conduits. Geomorphology 298, 86–106.
- Kavousi, A., Reimann, T., Liedl, R., Raeisi, E., 2020. Karst aquifer characterization by inverse application of MODFLOW-2005 CFPv2 discrete-continuum flow and transport model. J. Hydrol., 124922
- Klimchouk, A., 2004. Towards defining, delimiting and classifying epikarst: Its origin, processes and variants of geomorphic evolution. Speleogenesis Evol. Karst Aquifers 2 (1) 1-13
- Kovács, A., Perrochet, P., 2008. A quantitative approach to spring hydrograph decomposition. J. Hydrol. 352 (1–2), 16–29.
- Kresic, N., 2010. Types and classifications of springs. In: Groundwater hydrology of springs. Butterworth-Heinemann, pp. 31–85.
- Knöll, P., Zirlewagen, J., Scheytt, T., 2020. Using radar-based quantitative precipitation data with coupled soil-and groundwater balance models for stream flow simulation in a karst area. J. Hydrol., 124884
- Landrum, C., Castrignanò, A., Mueller, T., Zourarakis, D., Zhu, J., 2013. Landscape scale assessment of soil moisture variability using auxiliary sensing technologies and multivariate geostatistics. In: In Kentucky Water Resources Annual Symposium, p. (p. 22)
- Lastennet, R., Mudry, J., 1997. Role of karstification and rainfall in the behavior of a heterogeneous karst system. Environ. Geol. 32 (2), 114–123.

- Long, J., Gilmour, P., Witherspoon, P.A., 1985. A model for steady fluid flow in random three-dimensional networks of disc-shaped fractures. Water Resour. Res. 21 (8), 1105–1115.
- Long, A.J., 2009. Hydrograph separation for karst watersheds using a two-domain rainfall–discharge model. J. Hydrol. 364 (3–4), 249–256.
- MacQuown, W.C., Dobrovolny, E., 1968. Geologic map of the Lexington East quadrangle, Fayette and Bourbon Counties. Kentucky No. 683.
- Malago, A., Efstathiou, D., Bouraoui, F., Nikolaidis, N.P., Franchini, M., Bidoglio, G., Kritsotakis, M., 2016. Regional scale hydrologic modeling of a karst-dominant geomorphology: The case study of the Island of Crete. J. Hydrol. 540, 64–81.
- Massei, N., Wang, H.Q., Dupont, J.P., Rodet, J., Laignel, B., 2003. Assessment of direct transfer and resuspension of particles during turbid floods at a karstic spring. J. Hydrol. 275 (1–2), 109–121.
- Massei, N., Dupont, J.P., Mahler, B.J., Laignel, B., Fournier, M., Valdes, D., Ogier, S., 2006. Investigating transport properties and turbidity dynamics of a karst aquifer using correlation, spectral, and wavelet analyses. J. Hydrol. 329 (1–2), 244–257.
- Matthäi, S.K., Belayneh, M., 2004. Fluid flow partitioning between fractures and a permeable rock matrix. Geophys. Res. Lett. 31 (7).
- Milanović, P., 2014. Hydraulic properties of karst groundwater and its impacts on large structures. In H2Karst Research in Limestone Hydrogeology. Springer, Cham, pp. 19–48.
- Miller, R.D., 1967. Geologic map of the Lexington West quadrangle, Fayette and Scott Counties. Kentucky: US Geol. Survey Geol. Quad. Map GQ-600.
- Moody, L.F., 1944. Friction factors for pipe flow. Trans. Asme 66, 671-684.
- Moriasi, D.N., Arnold, J.G., Van Liew, M.W., Bingner, R.L., Harmel, R.D., Veith, T.L., 2007. Model evaluation guidelines for systematic quantification of accuracy in watershed simulations. Trans. ASABE 50 (3), 885–900.
- Munson, B.R., Okiishi, T.H., Huebsch, W.W., Rothmayer, A.P., 2013. Fluid mechanics. Wiley. Singapore.
- Neitsch, S.L., Arnold, J.G., Kiniry, J.R., Williams, J.R., 2011. Soil and water assessment tool theoretical documentation version 2009. Texas Water Resources Institute.
- Niswonger, R. G., Prudic, D. E., & Regan, R. S., 2006. Documentation of the unsaturatedzone flow (UZF1) package for modeling unsaturated flow between the land surface and the water table with MODFLOW-2005 (No. 6-A19).
- Ollivier, C., Mazzilli, N., Olioso, A., Chalikakis, K., Carrière, S.D., Danquigny, C., Emblanch, C., 2020. Karst recharge-discharge semi distributed model to assess spatial variability of flows. Sci. Total Environ. 703, 134368.
- Ou, G., Munoz-Arriola, F., Uden, D.R., Martin, D., Allen, C.R., Shank, N., 2018. Climate change implications for irrigation and groundwater in the Republican River Basin, USA. Clim. Change 151 (2), 303–316.
- Paylor, R., Currens, J.C., 2004. Royal Springs Karst Groundwater Travel Time Investigation. A report prepared for Georgetown Municipal Water and Sewer Service. Lexington. KY.
- Pétré, M.A., Rivera, A., Lefebvre, R., 2019. Numerical modeling of a regional groundwater flow system to assess groundwater storage loss, capture and sustainable exploitation of the transboundary Milk River Aquifer (Canada–USA). J. Hydrol. 575, 656–670.
- Phillips, J.D., Walls, M.D., 2004. Flow partitioning and unstable divergence in fluviokarst evolution in central Kentucky. Nonlinear Process. Geophys. 11 (3), 371–381.
- Pinault, J.L., Plagnes, V., Aquilina, L., Bakalowicz, M., 2001. Inverse modeling of the hydrological and the hydrochemical behavior of hydrosystems: Characterization of karst system functioning. Water Resour. Res. 37 (8), 2191–2204.
- Puckett, J., 2015. Qualitative and Quantitative Charachteristics of Fluvial Karst Features in the Cane Run Watershed.
- Qiu, H., Niu, J., Hu, B.X., 2019. Quantifying the integrated water and carbon cycle in a data-limited karst basin using a process-based hydrologic model. Environ. Earth Sci. 78 (11), 328.

- Rooij, R., Perrochet, P., Graham, W., 2013. From rainfall to spring discharge: Coupling conduit flow, subsurface matrix flow and surface flow in karst systems using a discrete–continuum model. Adv. Water Resour. 61, 29–41.
- Saltelli, A., Ratto, M., Andres, T., Campolongo, F., Cariboni, J., Gatelli, D., Saisana, M., Tarantola, S., 2008. Global sensitivity analysis: the primer. John Wiley & Sons.
- Sawyer, A.H., Zhu, J., Currens, J.C., Atcher, C., Binley, A., 2015. Time-lapse electrical resistivity imaging of solute transport in a karst conduit. Hydrol. Process. 29 (23), 4968–4976.
- Shoemaker, W.B., Cunningham, K.J., Kuniansky, E.L., Dixon, J., 2008. Effects of turbulence on hydraulic heads and parameter sensitivities in preferential groundwater flow layers. Water Resour. Res. 44 (3).
- Singh, V.P., 2012. Computer models of watershed hydrology. WRP.
- Simunek, J., Sejna, M., Van Genuchten, M.T., Šimunek, J., Šejna, M., Jacques, D. and Sakai, M., 1998. HYDRUS-1D. Simulating the one-dimensional movement of water, heat, and multiple solutes in variably-saturated media, version, 2.
- Snow, D.T., 1969. Anisotropie permeability of fractured media. Water Resour. Res. 5 (6), 1273–1289.
- Spangler, L.E., 1982. Karst hydrogeology of northern Fayette and southern Scott counties, Kentucky (Doctoral dissertation. University of Kentucky).
- Talarovich, S.G., Krothe, N.C., 1998. Three-component storm hydrograph separation of a karst spring contaminated by polychlorinated biphenyls in central Indiana. Environ. Geosci. 5 (4), 162–176.
- Taylor, C.J., 1992. Ground-water occurrence and movement associated with sinkhole alignments in the Inner Bluegrass Karst Region of central Kentucky (Doctoral dissertation. University of Kentucky).
- Thrailkill, J. and Gouzie, D.R., 1984. Discharge and travel time determinations in the Royal Spring groundwater basin, Kentucky.
- Thrailkill, J., Sullivan, S.B., Gouzie, D.R., 1991. Flow parameters in a shallow conduitflow carbonate aquifer, Inner Bluegrass Karst Region, Kentucky, USA. J. Hydrol. 129 (1–4), 87–108.
- Tibouo, N.T.F., 2016. Use and Evaluation of LiDAR for Mapping Sinkholes in Royal Spring Groundwater Basin (Doctoral dissertation. University of Kentucky Libraries).
- Tritz, S., Guinot, V., Jourde, H., 2011. Modelling the behaviour of a karst system catchment using non-linear hysteretic conceptual model. J. Hydrol. 397 (3–4), 250–262
- UKCAFE (University of Kentucky College of Agriculture Food and the Environment), 2011. Cane Run and Royal Spring watershed-based plan, version 5. EPA Project Number C9994861-06. In: Univ. Kentucky Coll. Agric. Food Environ. www.bae.uky.edu/CaneRun/PDFs/Cane_Run_WBP_2011.pdf. Accessed 6 Jan 2018.
- www.bae.uky.edu/CaneRun/PDFs/Cane_Run_WBP_2011.pdf. Accessed 6 Jan 2018. White, W.B., 1999. Conceptual models for karstic aquifers. Karst Model. 5, 11–16. White, W.B., 2002. Karst hydrology: recent developments and open questions. Eng. Geol.
- 65 (2–3), 85–105.
 Williams, P.W., 2008. The role of the epikarst in karst and cave hydrogeology: A review.
 Int. J. Speleol. 37 (1), 1.
- Int. J. Speleol. 37 (1), 1. Worthington, S.R.H., Ford, D.C., 2009. Self-organized permeability in carbonate aquifers.
- Groundwater 47 (3), 326–336.
- Worthington, S.R., 2007. Groundwater residence times in unconfined carbonate aquifers.

 J. Cave Karst Studies 69 (1), 94–102.
- Xu, Z., Bassett, S.W., Hu, B., Dyer, S.B., 2016. Long distance seawater intrusion through a karst conduit network in the Woodville Karst Plain, Florida. Scientific Reports 6 (1), 1–10.
- Zhu, J., Currens, J.C., Dinger, J.S., 2011. Challenges of using electrical resistivity method to locate karst conduits – a field case in the Inner Bluegrass Region, Kentucky. J. Appl. Geophys. 75 (3), 523–530.
- Zimmerman, R.W., Yeo, I.W., 2000. Fluid flow in rock fractures: From the Navier-Stokes equations to the cubic law. Geophysic.